iScience

CellPress
OPEN ACCESS

Article

Origin and Lineage Plasticity of Endogenous Lacrimal Gland Epithelial Stem/Progenitor Cells

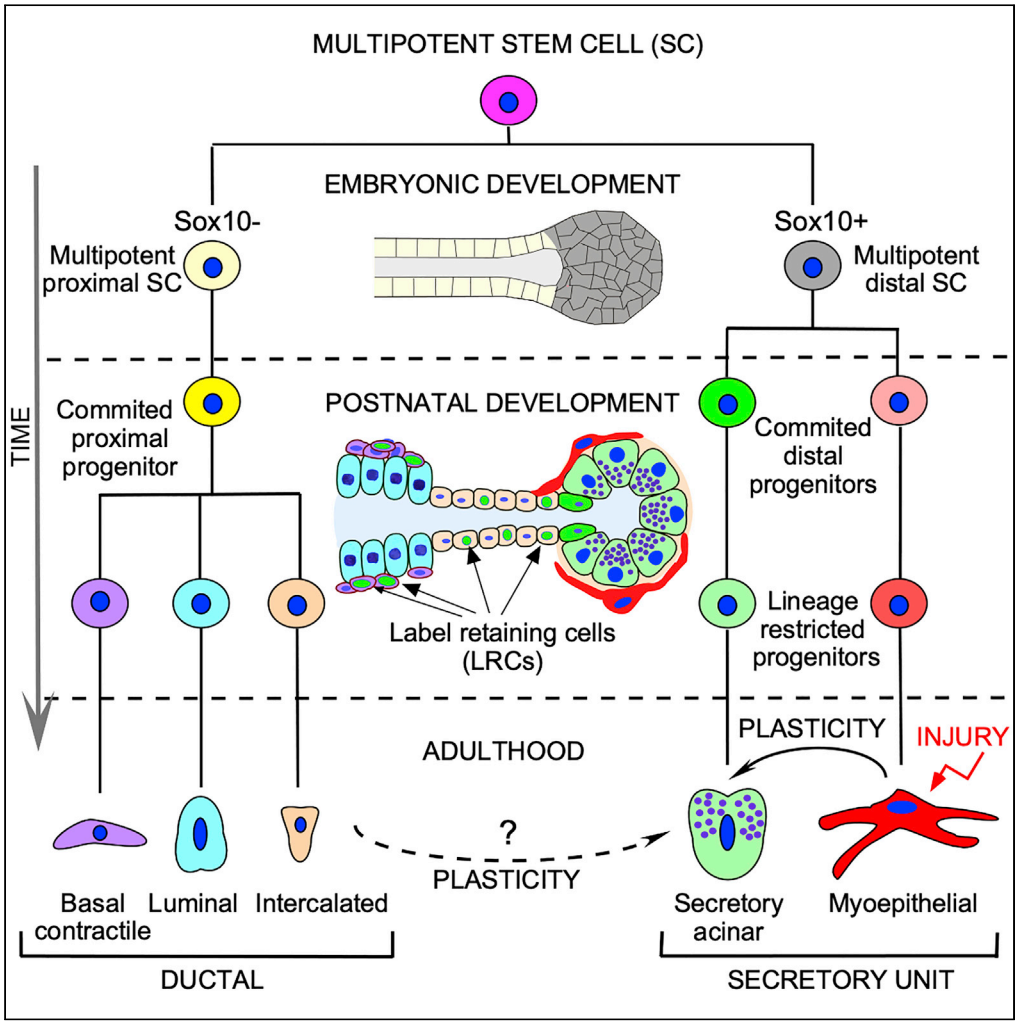

Liana Basova, Geraint J. Parfitt, Alex Richardson, ..., Nick Di Girolamo, James V. Jester, Helen P. Makarenkova

hmakarenk@scripps.edu

HIGHLIGHTS

Multipotent stem cells differentiate into distal Sox10+ and proximal Sox10− lineages

Lineage-restricted progenitor cells sustain the long-term lacrimal gland maintenance

Label-retaining cells are localized in the intercalated ducts and excretory ducts

Some cell lineages in the adult lacrimal gland retain plasticity

Basova et al., iScience *23*, 101230
June 26, 2020
https://doi.org/10.1016/j.isci.2020.101230

iScience

CellPress
OPEN ACCESS

Article

Origin and Lineage Plasticity of Endogenous Lacrimal Gland Epithelial Stem/Progenitor Cells

Liana Basova,[1,8] Geraint J. Parfitt,[2,3,4,8] Alex Richardson,[5] Vanessa Delcroix,[1] Takeshi Umazume,[1] Daniel Pelaez,[6] David T. Tse,[6] Ivo Kalajzic,[7] Nick Di Girolamo,[5] James V. Jester,[4] and Helen P. Makarenkova[1,9,*]

SUMMARY

The lacrimal gland (LG) is an exocrine organ responsible for the secretion of aqueous tear film. Regenerative and stem cell therapies that target LG repair are coming to the fore, although our understanding of LG cell lineage hierarchy is still incomplete. We utilize the analysis of label-retaining cells (LRCs) and genetic lineage tracing to define LG cell lineage hierarchy. Our study suggests that embryonic LG contains unique long-lived multipotent stem cells that give rise to all postnatal epithelial cell types. Following birth, lineages become established and the fate of progenitor cell descendants becomes restricted. However, some cell lineages retain plasticity after maturation and can trans-differentiate into other cell types upon injury. The demonstration that the LG contains progenitor cells with different levels of plasticity has profound implications for our understanding of LG gland function in homeostasis and disease and will be helpful for developing stem cell-based therapies in the future.

INTRODUCTION

Approximately 5 million Americans older than 50 years suffer from dry eye disease, with a significant number of cases linked to decreased tear production from the lacrimal gland (LG), an exocrine organ responsible for secreting the aqueous layer of the tear film (Khanal et al., 2009; Wuidart et al., 2018). Treatments to reduce tear loss for aqueous deficient dry eye disease (ADDE) include anti-inflammatory drugs, artificial tears, or punctal occlusion (Hamano, 2002; Roberts et al., 2007; Rouen and White, 2018; Tan et al., 2018). However, a major limitation of these therapies is that they treat the symptoms of ADDE, rather than the underlying etiology. Regenerative therapies that target LG repair, or the development of bioengineered tissues, have been recently reported (Gromova et al., 2017; Hirayama et al., 2013), although our understanding of LG biology is still incomplete. For example, it is not known how different cell populations arise during development and how they are maintained throughout life, and the identification and functional analysis of LG stem and progenitor cells has yet to be carried out. When this knowledge is translated to the clinic, it will enhance regenerative approaches that are currently being undertaken (Basova et al., 2017; Gromova et al., 2017; Hirayama et al., 2013).

Murine LG development begins at embryonic day (E) 13.5, as an outgrowth of conjunctival tissue that progressively elongates toward the ear (Kuony and Michon, 2017; Makarenkova et al., 2000). The primitive gland undergoes branching at E16.5 to form the intra- and extra-ocular structures (Garg and Zhang, 2017). Branching continues during both embryonic and post-natal development, and the gland becomes functionally mature at approximately postnatal day (P) 30 (Wang et al., 1995). Recently, embryonic lineage analysis using the constitutive K14-Cre43 (also known as Tg(KRT14-cre)43Smr) mouse line (Wuidart et al., 2016) suggested that LG morphogenesis follows a similar developmental process to other branched organs (prostate and mammary gland), making the LG a fitting model to study general glandular development (Kuony and Michon, 2017). Furthermore, others (Farmer et al., 2017) have also attempted to follow the epithelial cell lineage during LG development using inducible mouse lines; however, clonal analysis and long-term cell fate mapping was not performed in this study.

In both mice and humans, the adult mammalian LG contains both mesenchymal and epithelial cells, with the latter composed of three major lineages: the acinar cells, ductal cells, and myoepithelial cells (MECs) (Makarenkova and Dartt, 2015; Zouchri and Makarenkova, 2015; Zoukhri, 2006). MECs express α-smooth muscle actin (αSMA) and contract to modulate the secretory function of the acinar cells (Abe

[1]Department of Molecular Medicine, The Scripps Research Institute, 10550 North Torrey Pines Road, La Jolla, CA 92037, USA

[2]School of Optometry and Vision Sciences, Cardiff University, Maindy Road, Cardiff CF24 4HQ, UK

[3]European Cancer Stem Cell Research Institute, Cardiff University, Maindy Road, Cardiff CF24 4HQ, UK

[4]The Gavin Herbert Eye Institute, University of California, Irvine, CA 92697, USA

[5]Department of Ophthalmology, School of Medical Sciences, University of New South Wales, Sydney, NSW 2052, Australia

[6]Department of Ophthalmology/Bascom Palmer Eye Institute, Miami, FL, USA

[7]Reconstructive Sciences Center for Regenerative Medicine and Skeletal Development, University of Connecticut (UCONN) Health, Farmington, CT, USA

[8]These authors contributed equally

[9]Lead Contact

*Correspondence: hmakarenk@scripps.edu

https://doi.org/10.1016/j.isci.2020.101230

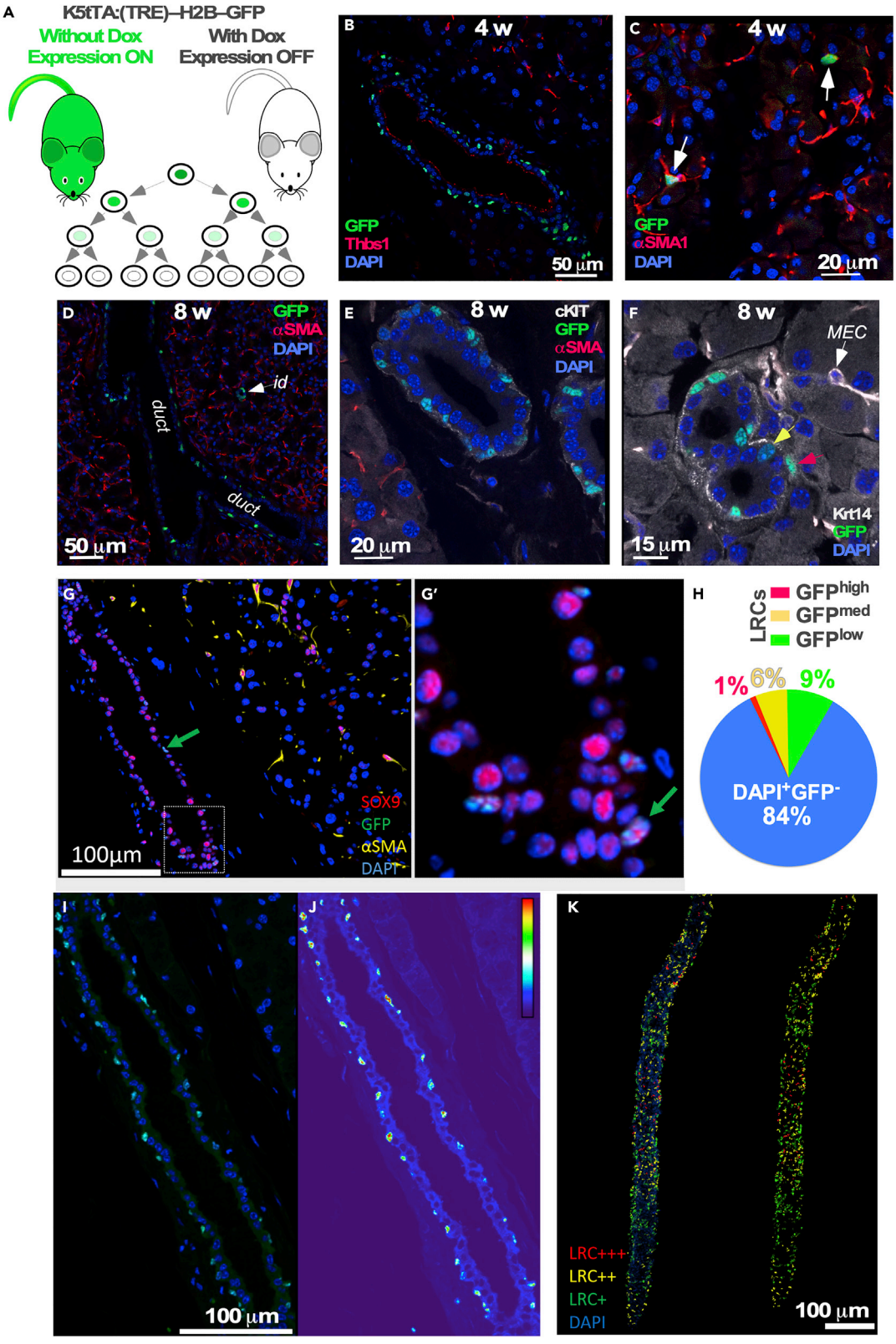
A
K5tTA:(TRE)–H2B–GFP
Without Dox
Expression ON
With Dox
Expression OFF
B
4 w
GFP
Thbs1
DAPI
50 μm
C
4 w
GFP
αSMA1
DAPI
20 μm
D
8 w
GFP
αSMA
DAPI
id
duct
duct
50 μm
E
8 w
cKIT
GFP
αSMA
DAPI
20 μm
F
8 w
MEC
Krt14
GFP
DAPI
15 μm
G
G′
SOX9
GFP
αSMA
DAPI
100μm
H
LRCs
GFPhigh
GFPmed
GFPlow
1%
6%
9%
DAPI+GFP-
84%
I
J
100 μm
K
LRC+++
LRC++
LRC+
DAPI
100 μm

Figure 1. Krt5^{+} Label-Retaining Cells (LRCs) Reside in the Ductal Epithelium

Twelve LGs per time point have been analyzed.

(A) Schematic of the experimental approach.

(B) After 30 days of doxycycline (DOX) administration labeled cells (green) were found in the basal layer of the ducts. They were not located in luminal cells (luminal cells were identified by Thrombospondin-1 antibody staining: red).

(C) GFP-labeled cells (green) were also found in a small subset of MECs marked by anti-αSMA staining (red).

(D–G) (D) After 8 weeks of doxycycline chase, LRCs (green) are found only in the basal ductal (*duct*) cells and intercalated duct cells (*id,* white arrow). Basal ductal cells also expressed c-kit (E: gray, also see Figure S2), Krt14 (F: gray, also see Figure S3), and Sox9 (G, G′: green arrows).

(H–K) LRCs exhibited variations in GFP fluorescence intensities. LRCs and other ductal cells were quantified on 3D reconstructions generated by immunofluorescence tomography. (H) Quantification of LRCs with different fluorescence intensities. (I–K) An index of label retention was used to visualize the range of GFP expression within cells of the reconstructed images. (I and J) Examples of single sections though LG duct. (K) Reconstraction of LG ducts. Cells were grouped according to level of GFP expression and are represented as high level, red (LRC^{+++}); medium level, yellow (LRC^{++}); low level, green (LRC^{+}); and no GFP expression, blue (non-LRC).

See also Figures S1–S3.

et al., 1981; Avci et al., 2012; Dartt, 2009; Faraldo et al., 2005; Gudjonsson et al., 2005; Hawley et al., 2018; Raubenheimer, 1987; Schon et al., 1999). The secretory acini are connected to ducts, which are composed of a basal and a luminal layer, that modify tear composition before it is secreted onto the ocular surface (Makarenkova and Dartt, 2015; Raubenheimer, 1987).

We have recently demonstrated that a population of c-kit^{+}dim/EpCAM^{+}/Sca1^{-}/CD34^{-}/CD45^{-} cells displayed the greatest number of progenitor hallmarks, which reinstated LG function following grafting into a damaged recipient gland (Gromova et al., 2017). Although analysis of stem cell (SC) localization and function has been performed in mammary (Rios et al., 2014; Shackleton et al., 2006; Visvader and Stingl, 2014) and salivary glands (Chibly et al., 2014; Zhang et al., 2014), the study of stem and progenitor cells in the LG is incomplete. There are two competing hypotheses regarding the origin of stem/progenitor cells in adult LGs: one postulates that a common multipotent (able to give rise to all epithelial lineages) stem/progenitor cell exists, whereas the second proposes that unipotent acinar, ductal, and MEC lineages are derived from lineage-specified SCs (Makarenkova and Dartt, 2015; Zoukhri and Makarenkova, 2015).

In the current study, we address how cell lineages are established in the adult LGs and whether multipotent or unipotent SCs exist during postnatal development, homeostasis, and regeneration. To achieve this, we combined lineage tracing in specific Cre reporter mouse strains (Krt14, Runx1, and αSMA) with *in vivo* analysis of infrequently dividing cells using a histone 2B (H2B)-GFP label retention system (Parfitt et al., 2015) expressed under control of the keratin 5 (Krt5) promoter. We established that the embryonic LG epithelium contains a unique long-lived cell population composed of undifferentiated, multipotent. and highly plastic progenitor cells that give rise to all postnatal epithelial cell types. Furthermore, our study demonstrates that LG morphogenesis during early postnatal development is driven by long-lived multipotent and unipotent embryonic progenitor cells, whereas the adult LG is maintained by long-lived and short-lived unipotent lineage-restricted stem/progenitor cells. These cells may contribute to LG renewal during homeostasis and/or regeneration. We also show that lineage-specific MECs retain a certain level of plasticity in the adult LG and are able to trans-differentiate into acinar cells following LG injury. The longevity of the unipotent lineage-restricted cells and their ability to participate in tissue regeneration suggests the universal plasticity of these and possibly other cell types in the LG. Our study suggests a model where injury/acute inflammation activates proliferation of the existing lineage-restricted progenitors, which is then continued by slowly proliferating long-term common reserve progenitor cells and their progenies. Our findings provide important new concepts, while revealing differences in the homeostatic and regenerative potential of stem and progenitor cells in LGs.

RESULTS

Slow-Cycling Label-Retaining Cells Are Localized in the Basal Layer of the Lacrimal Gland Intra- and Interlobular Ducts and Intercalated Ducts

Two unique properties of SCs are quiescence (label retention hypothesis) and longevity (the capacity to form long-lived clones). The ability to retain a DNA label is a common feature among SCs from several adult tissues including cornea, sweat, salivary, and lacrimal glands (Chibly et al., 2014; Emmerson and Knox, 2018; Leung et al., 2013; You et al., 2011; Zhao et al., 2009). To detect label-retaining cells (LRCs) in the LG, we employed the H2B-GFP pulse-chase labeling system (Figure 1A). After the 28-day pulse phase, H2B-GFP/K5tTA mice were fed a doxycycline-containing diet for 30 days (4 weeks) and 56 days (8 weeks) to

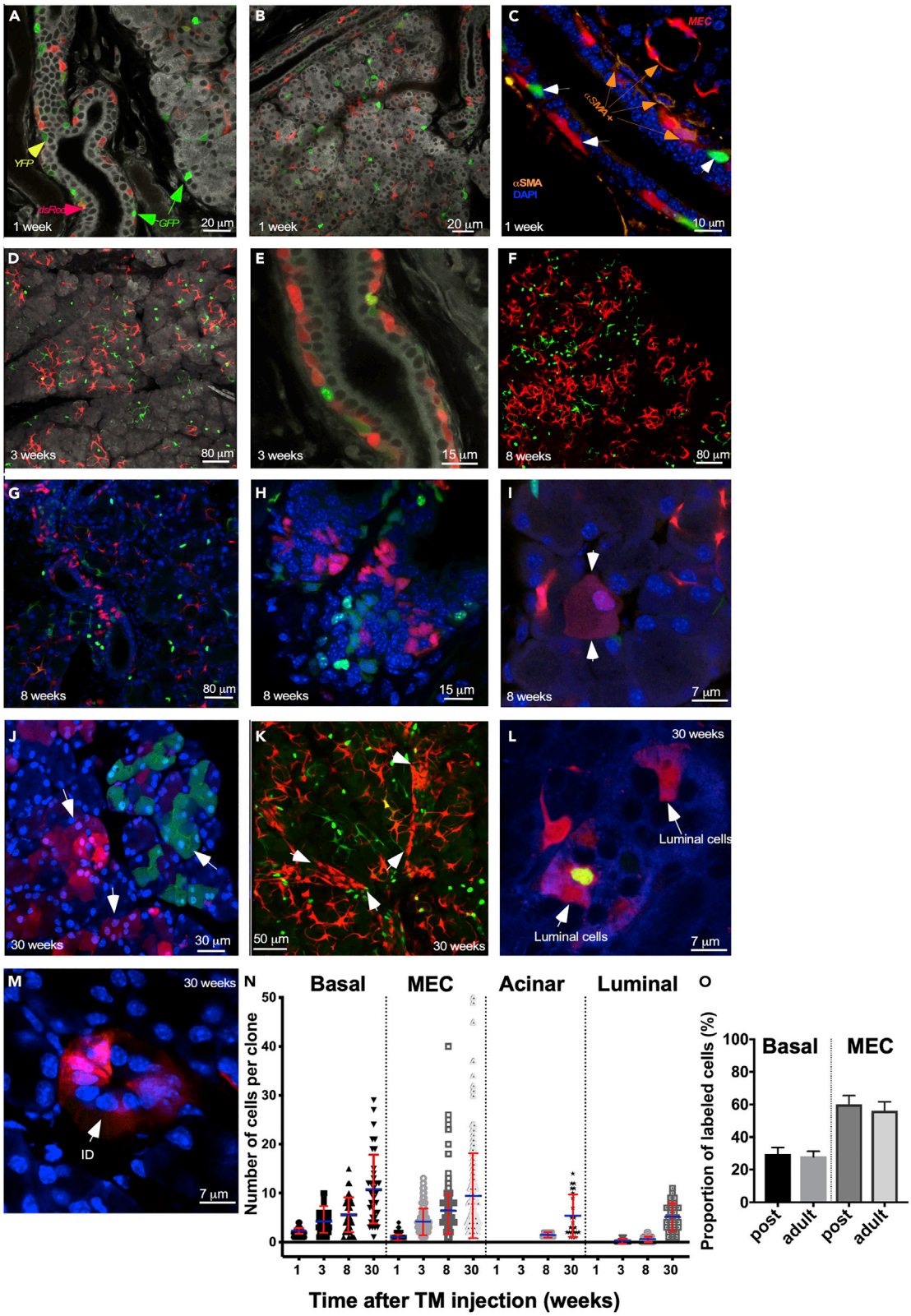
A
YFP
dsRed
GFP
1 week
20 μm
B
1 week
20 μm
C
MEC
αSMA+
αSMA
DAPI
1 week
10 μm
D
3 weeks
80 μm
E
3 weeks
15 μm
F
8 weeks
80 μm
G
8 weeks
80 μm
H
8 weeks
15 μm
I
8 weeks
7 μm
J
30 weeks
30 μm
K
50 μm
30 weeks
L
30 weeks
Luminal cells
Luminal cells
7 μm
M
30 weeks
ID
7 μm
N
Basal
MEC
Acinar
Luminal
Number of cells per clone
0
10
20
30
40
50
1 3 8 30 1 3 8 30 1 3 8 30 1 3 8 30
Time after TM injection (weeks)
O
Proportion of labeled cells (%)
0
20
40
60
80
100
Basal
MEC
post
adult
post
adult

Figure 2. Lineage Tracing of Krt14^{+} Cells in the LGs of the *Krt14^{CreERT2}:R26-Confetti* Mice (Also See Figure S4)

(A–L) TM was administrated at P7, and LGs were analyzed 1 week (A–C), 3 weeks (D and E), 8 weeks (F–I), and 30 weeks (J–L) later.

(A and B) 1-week chase: labeled cells were found in the basal layer of excretory ducts (A: GFP is nuclear [green, green arrows], YFP is cytoplasmic [pale green, yellow arrows], dsRed is cytoplasmic [red, red arrows]) and majority of MECs. Note: No labeling was observed in acinar cells.

(C) 1-week chase: immunostaining of LG for αSMA reveals a subset of αSMA^{+} (αSMA^{+}, orange arrows) cells within the basal layer of excretory ducts. However, some of basal ductal cells were αSMA^{-} (white arrows, also see Figure S5).

(D and E) Analysis of labeled MECs induced by tamoxifen administration at P7 after a 3-week chase. Clonal expansion of MECs (D) and basal ductal cells is apparent after a 3-week (E) chase period.

(F–I) Analysis of labeled MECs induced by tamoxifen administration at P7 after an 8-week chase. Clonal expansion of MECs (F) and basal ductal cells (G and H) is observed. (I) After an 8-week chase, rare single acinar cells were observed (white arrows).

(J) Acinar cells formed small clones after a 30-week chase (white arrows).

(K–M) (K) Expansion of basal ductal cells (white arrows) and MECs after a 30-week chase. Labeled luminal cells in the excretory ducts (L) and intercalated ducts (M) were observed after a 30-week chase.

(N) Clonal expansion of Krt14^{+} cells during postnatal development and homeostasis. LGs obtained from *Krt14^{CreERT2}:R26-Confetti* male mice were analyzed at different time points (3–5 glands per time point). Clonal analysis was performed within each cellular compartment. Thus, ductal cells were classified as luminal or basal based on their position, morphology, and nuclear shape. Clonal size was determined separately within each of these compartments (for example, measured clone sizes in each ductal compartment include only basal cells or only luminal cells). Clonal size is represented by the number of cells per clone ± SD, $p < 0.05$, one-way ANOVA. Mean is blue, SD is red.

(O) Comparison of cell-labeling efficiency in the LGs during postnatal development and adulthood. The proportion of labeled basal ductal and MECs was compared with unlabeled basal ductal or MECs cells. Cells were labeled in postnatal development at P7 or in adulthood at P30 (percent of labeled cells ± SD; basal ducal cells $p = 0.2531$, MECs $p = 0.1044$; two-tailed t test). No significant difference between number of labeled cells in postnatal development and adulthood was observed. See also Figures S4–S6.

shut off H2B-GFP expression and dilute the GFP by 50% with every cell division (Figure 1A). Before the chase (Figures S1A–S1C), GFP was found in almost all MECs (Figure S1E, MEC: 92.5% ± 4.3%) and intercalated ducts (Figure S1E, ID: 98.1% ± 2.0%) and in the majority of basal ductal cells (Figure S1E, BD: 89.5% ± 9.3%). A small number of GFP-labeled luminal ductal cells was also found (Figures S1E and S1E′, LUM: 3.3% ± 2.7%). No labeling of acinar cells was detected (Figures S1A–S1C and S1E). Following a 4-week chase, LRCs were observed in the basal epithelium of all inter- and intra-lobular ducts (35% ± 5%), as determined by Thrombospondin-1 (Thsp1) immunostaining (Figure 1B), which labels luminal ductal cells (Gromova et al., 2017), and in MECs (4.1% ± 0.9%), as determined by αSMA expression (Figure 1C, white arrows). Observing a subpopulation of LRCs within MECs suggests the presence of slow-cycling progenitor cells within the MEC lineage.

After an 8-week chase there was complete depletion of the GFP signal in MECs, and LRCs were only found in a subset of basal cells of the intra-lobular, excretory, and intercalated ducts (Figure 1D). These ductal LRCs expressed Krt5 (Figure S1F), c-kit (Figures 1E and S2), Krt 14 (Figures 1F, S1G, S1H, and S3), and the embryonic progenitor cell marker Sox9 (Figures 1G and 1G′). Sox9 expression was observed in all ductal and MEC cells of adult glands (Figures 1G and 1G′), whereas Sox10 expression, similar to embryonic LG (Chen et al., 2014), was observed in the distal LG compartments: acinar cells and MECs (Figures S1I–S1K).

Following the chase periods, we quantified the fluorescence intensity of LRCs using 3-dimensional reconstructions of immunofluorescence tomography scans (n = 3, 323 ± 38 μm^{3}) (Figures 1H–1K) and cells were grouped based on their GFP expression (see Methods): high level of GFP expression, red (LRC^{+++}); medium level, yellow (LRC^{++}); low level, green (LRC^{+}); and no GFP expression, blue (non-LRC) (Figures 1I–1K). Using this system of indexing cells, we observed 1% ± 0.28% LRC^{+++}, 6% ± 0.13% LRC^{++}, and 9% ± 0.2% LRC^{+} from the total cells within a field of view (Figure 1H). Cells with the highest GFP expression (LRC^{+++}) following the 8-week chase were deemed to be quiescent stem/progenitor population. These data indicate that there are at least two sources of slow-cycling LRCs in the LG: within the basal cells of inter- and intra-lobular ducts and a subset of cells in the intercalated ducts.

Lineage Tracing Using the Confetti Mouse Demonstrates the Existence of LG Krt14^{+} Multipotent Progenitor Cells during Early Postnatal Development

Analysis of Krt5 and Krt14 expression patterns (Figure S4) demonstrated that although their expression pattern may not completely overlap (Figure S4), both keratins were expressed in the same cellular compartments of LG: MEC and basal ductal cells. As Krt5 and Krt14 were expressed in the same cellular compartments, we utilized the K14^{CreERT2}-Confetti mouse to trace the Krt14 cell lineage. Mice were administered tamoxifen (TM) during early postnatal development (at P7), and their LGs were examined 1, 3, 8, and 30 weeks later (Figure 2). After a 1-week chase, Krt14^{+} cells were found in the basal layer of inter- and

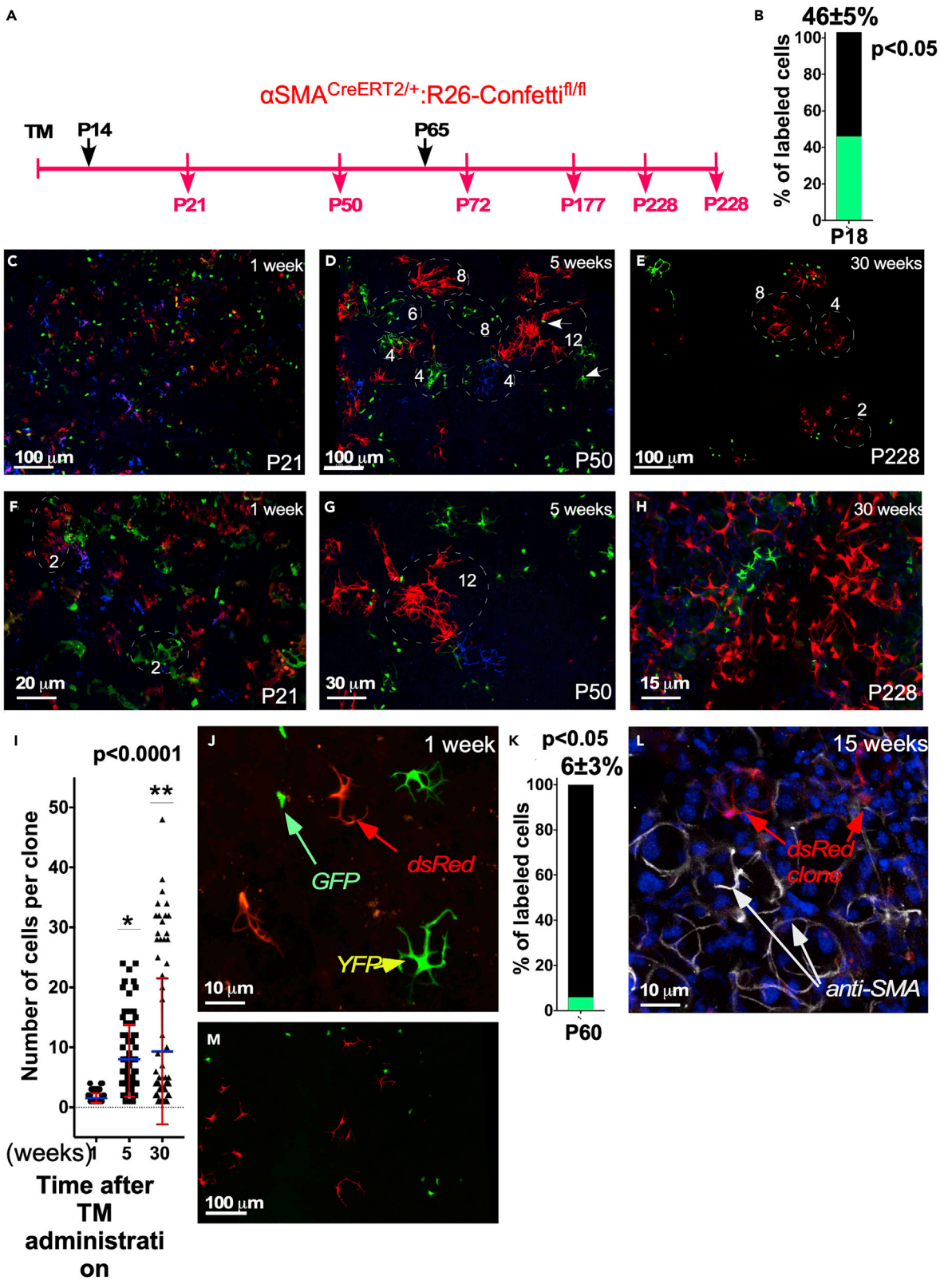
A
αSMA^CreERT2/+:R26-Confetti^fl/fl
TM
P14
P21
P50
P65
P72
P177
P228
P228
B
46±5%
p<0.05
% of labeled cells
P18
C
1 week
100 µm
P21
D
5 weeks
100 µm
P50
E
30 weeks
100 µm
P228
F
1 week
20 µm
P21
G
5 weeks
30 µm
P50
H
30 weeks
15 µm
P228
I
p<0.0001
Number of cells per clone
(weeks)
Time after TM administration
J
1 week
GFP
dsRed
YFP
10 µm
M
100 µm
K
p<0.05
6±3%
% of labeled cells
P60
L
15 weeks
dsRed clone
anti-SMA
10 µm

Figure 3. MEC Cell Lineage Tracing in the LG of the *SMA^{CreERT2}:R26-Confetti* Mice

(A) Schematic diagram of the experimental design. *SMA^{CreERT2}:R26-Confetti* mice were injected with TM at P14, and LGs were analyzed 1, 5, and 30 weeks later. Similarly, adult mice were injected with TM at P65, and LGs were excised and studied 1 and 15 weeks later.

(B) Labeling efficiency after TM administration at P14 (determined in 1 week after TM injection).

(C and F) Mosaic labeling of MECs 1 week after TM administration. (C) Low magnification image showing many labeled MECs. MECs still have an immature phenotype, i.e., their processes are short and thick (F).

(D, E, G, and H) (D and G) After 5 weeks MECs form well-distinguishable clones. Thirty weeks later MEC clone size varies from being small (E and H, green clone), i.e., consisting of 1–5 cells, to large (H), consisting of 32–50 cells (red clone), suggesting the existence of short- and long-term proliferating cells within the MEC lineage.

(I) Quantification of MEC clones after TM administration at P14. Results show mean ± SD, $p < 0.0001$, as determined by the Wilcoxon-signed rank test.

(J–M) (J) MECs labeled at P65 show mature phenotype but low labeling efficiency (K) (GFP [bright green], nuclear; YFP [green], cytoplasmic; and dsRed [red], cytoplasmic), as determined at 1 week after TM administration. 15 weeks after TM administration only small clones consisting of 1–4 cells were detected in adult *SMA^{CreERT2}:R26-Confetti* mice (L and M). MECs in (L) were immunostained for αSMA.

intra-lobular excretory and intercalated ducts, and MECs (Figures 2A and 2B). Co-immunostaining with αSMA antibody revealed that in addition to MECs, a subset of αSMA$^+$ cells was present within the basal layer of excretory interlobular ducts (Figure 2C, orange arrows, Figure S5), whereas some of basal ductal cells were αSMA$^-$ (white arrows). Phalloidin staining supported this observation and showed that some cells in the basal layer of LG ducts contain filamentous actin (Figures S6A and S6B). Large amount of filamentous actin was also present in the apical parts of the ductal luminal cells (Figures S6A and S6B). Thus, luminal and some of the basal ductal cells may have a contractile function to assist in tear release.

Analysis of Krt14-labeled cells after a 3-week chase detected clonal expansion of MECs (Figures 2D), 4.3 ± 0.5 cells per clone (Figure 2N). After an 8- (Figures 2F and 2N) and 30-week chase (Figure 2N), the number of MECs in clones continue to increase (6.1 ± 3.5 cells per clone after 8-weeks of chase and 14.6 ± 16.1 cells per clone after a 30-week chase). This finding suggests that MEC population may contain a subset of long-lived proliferating progenitor cells. Krt14$^+$ clones were also found within the basal layer of ducts at 3 weeks (Figures 2E and 2N), 4.3 ± 2.1 cells per clone; 8 weeks (Figures 2G, 2H, and 2N), 5.6 ± 3.6 cells per clone; and 30 weeks of chase (Figures 2N), 10.8 ± 7.4 cells per clone, also suggesting that the basal ductal cell population may harbor long-lived progenitors.

We did not observe labeling of acinar cells before an 8-week chase, at this stage only detecting rare single Krt14$^+$ acinar (1.4 ± 0.5 cells per clone; Figures 2I and 2N) cells. Thirty-weeks after TM administration, we observed small numbers of acinar cell clones (5.2% ± 4.3%; Figures 2J and 2N). Similarly, a few single labeled luminal ductal cells were found after a 3- and 8-week chase (Figure 2N), whereas after a 30-week chase labeled luminal cells formed small clones (5.0 ± 2.8 cells per clone) (Figures 2L and 2N). Labeling of intercalated duct cells (2.2% ± 0.8%) was observed only after a 30-week chase (Figure 2M). The rare labeling of acinar and luminal ductal cells in the intra-lobular and intercalated ducts could be explained by the small number of labeled bi- or multipotent stem/progenitor cells present in the LG during postnatal development, low cell replacement rate in these lineages, or Krt14 lineage restriction during early postnatal LG development.

Interestingly, TM administration to adult (cells were labeled at P30 and analyzed at P90) Krt14^{CreERT2}:Confetti mice revealed labeling of only MECs and basal ductal cells. No luminal ductal or acinar cells were observed at 8- or 30-week chase times. A comparison of the proportion of labeled basal ductal and MECs in the LG of mice labeled at P7 and P30 showed that cells in basal ductal and MEC compartments of young and adult mice were labeled with similar efficiency (Figure 2O). This suggests that the efficiency of TM-induced reporter expression during LG postnatal development and adulthood was similar.

Analysis of SMA$^+$ MECs Reveal Their Proliferation and Self-Renewal during Postnatal Development and Early Adulthood

As Krt14 expression was found in MECs, we could not rule out the possibility that the MEC lineage contains multipotent SCs capable of occasionally differentiating into acinar or ductal cells. We administered TM to *SMA$^{CreERT2:}$R26-Confetti* mice at P14 (when MECs differentiate) and analyzed their LGs following various chase periods (Figure 3A). Labeling efficiency using R26-Confetti during postnatal development was determined as 46% ± 5%, $p < 0.05$ (Figure 3B). Clonal analysis following a 1-week chase period revealed mosaic labeling of single cells, with rare clones consisting of 1–4 cells (1.5 ± 0.7, $p < 0.0001$) (Figures 3C, 3F, and 3I). Analysis of LGs 5 weeks after TM administration demonstrated clonal expansion of MEC with the largest

clones consisting of 12–18 cells (7.7 ± 5.8, $p < 0.0001$) (Figures 3D, 3G, and 3I) and with no labeling apparent on other cell types. Analysis of MEC clones following a 30-week chase period showed a variation of cell numbers in clones and the simultaneous existence of small (1–4 cells) (Figures 3E, 3H and 3I) and large (12–34 cells) clones (12 ± 13.4, $p < 0.0001$) (Figures 3H and 3I). These findings, combined with Krt14 labeling and the detection of a subset of relatively slowly proliferating MECs, suggest that the MEC lineage may contain long-lived unipotent stem/progenitor cells capable of renewing the MEC pool throughout the organism's life.

MECs were also labeled in adult LGs at P65 and analyzed 1, 15, and 30 weeks later (Figures 3J–3L). In the adult LG only 6% ± 3% cells were labeled (Figure 3K), which allowed us to clearly distinguish each clone from its neighbors. After a 15-week chase only small clones containing 2–4 cells were detected (Figure 3L). However, labeled MECs were still found even after a 30-week chase (Figure 3M), again implying that the adult MEC lineage contains long-lived cells.

To determine whether embryonic MECs contribute to other cell lineages in adult LGs, pregnant *SMA-$^{CreERT2/+}$:R26-Tomato$^{fl/fl}$* females were injected with TM at E14.5–E15.0 and LGs were harvested following chase periods between 2 and 60 days (Figure 4A). At E17.0 (2-day chase), embryonic LGs demonstrated that SMA-expressing MEC progenitors originate from the external layer of cells within the developing epithelial bud (Figures 4B and 4C). All MEC progenitors typically had a cuboidal shape and did not display membrane processes (Figures 4B and 4C). At this stage labeling efficiency was high (98% ± 1.9%) as observed by immunostaining LGs at E19 with an αSMA antibody (Figures 4D–4G). Following a 4-day chase at E19, differentiating MECs formed small membrane protrusions (Figures 4I and 4J). Similar to LG epithelial cells, MEC progenitors expressed Pax6 (Figures 4H–4J, red arrows). During early postnatal development MECs continue to differentiate and form longer processes by P30 (Figure 4K); however, they remain to be associated with the maturating acinar component of the gland, as shown by labeling of ductal (Panx1) and acinar (Claudin1) compartments of the LG (Figures 4L and 4M). By the end of postnatal development, at approximately P30, MECs were fully differentiated into stellate cells with several long processes surrounding epithelial acini, and by P60, they form a continuous MEC network (Video S1).

Comparison of genetically labeled MECs in the αSma$^{CreERT2/+}$:Rosa26-Tomato$^{fl/fl}$ (C57BL/6 Strain) with the MECs stained with αSMA antibody in wild-type C57BL/6 strain showed similar MEC distribution and appearance (not shown). Next, we determined whether MECs proliferate during postnatal development. Cells were labeled at P10/11, and LGs were analyzed at P20. Proliferating cells were detected using an anti phospho-histone H3 antibody (Figures 4N and 4O). We found proliferating cells in all epithelial compartments (Figures 4N–4P), including acinar cells (3.7 ± 1.0), ductal cells (2.1 ± 0.9), and MECs (4.2 ± 2.2) of the LG and mesenchyme (1.5 ± 0.8).

We also determined whether there is an increase in the number of MECs compared with the number of nuclei during LG development and maturation. Cells were labeled by injecting mice with TM at P10/11 or P27/28, and the number of labeled MECs within at least 1,000 cells (number of labeled MECs per 1,000 nuclei) was calculated at P14 and P40 or P30, P60, and P120 correspondingly (Figures 4Q–4T and 4U). We found a substantial and statistically significant increase in MEC number during postnatal development and in early adulthood (Figures 4T and 4U); however, between P60 and P120 the number of MECs remained the same (Figure 4U). Thus, we established that SMA$^+$ MECs proliferate but do not differentiate into any other cell types, suggesting that the SMA$^+$ MEC lineage is distinct and established early in embryonic development.

The Lacrimal Gland of Adult Mice Contains αSMA-Negative Stem/Progenitor Cells Able to Differentiate into αSMA-Positive MECs

Our data support the hypothesis that under homeostatic conditions the αSMA$^+$ MEC lineage in the LG is a distinct lineage, which is maintained by proliferating αSMA$^+$ progenitors. To determine whether αSMA$^+$ MEC lineage is really a distinct cell lineage in the LG thoughout whole mouse lifespan, we labeled cells by injecting *αSMA$^{CreERT2/+}$:R26-Tomato$^{fl/fl}$* mice with TM at P14/15 and followed the MEC lineage for up to 24 months. We found that at P21 almost all labeled (dsRed$^+$) MECs were also stained with αSMA antibody (99.3 ± 0.7, $p < 0.05$, $n = 15$) (Figures 5A–5C and 5J). However, we observed a significant decrease in proportions of the αSMA$^+$/dsRed$^+$ MECs (66.8 ± 11.6, $p < 0.05$, $n = 12$) after a 6- and (51.3 ± 5.7, $p < 0.05$, $n = 12$) 24-month chase within the population of MECs stained with αSMA antibody (Figure 5J).

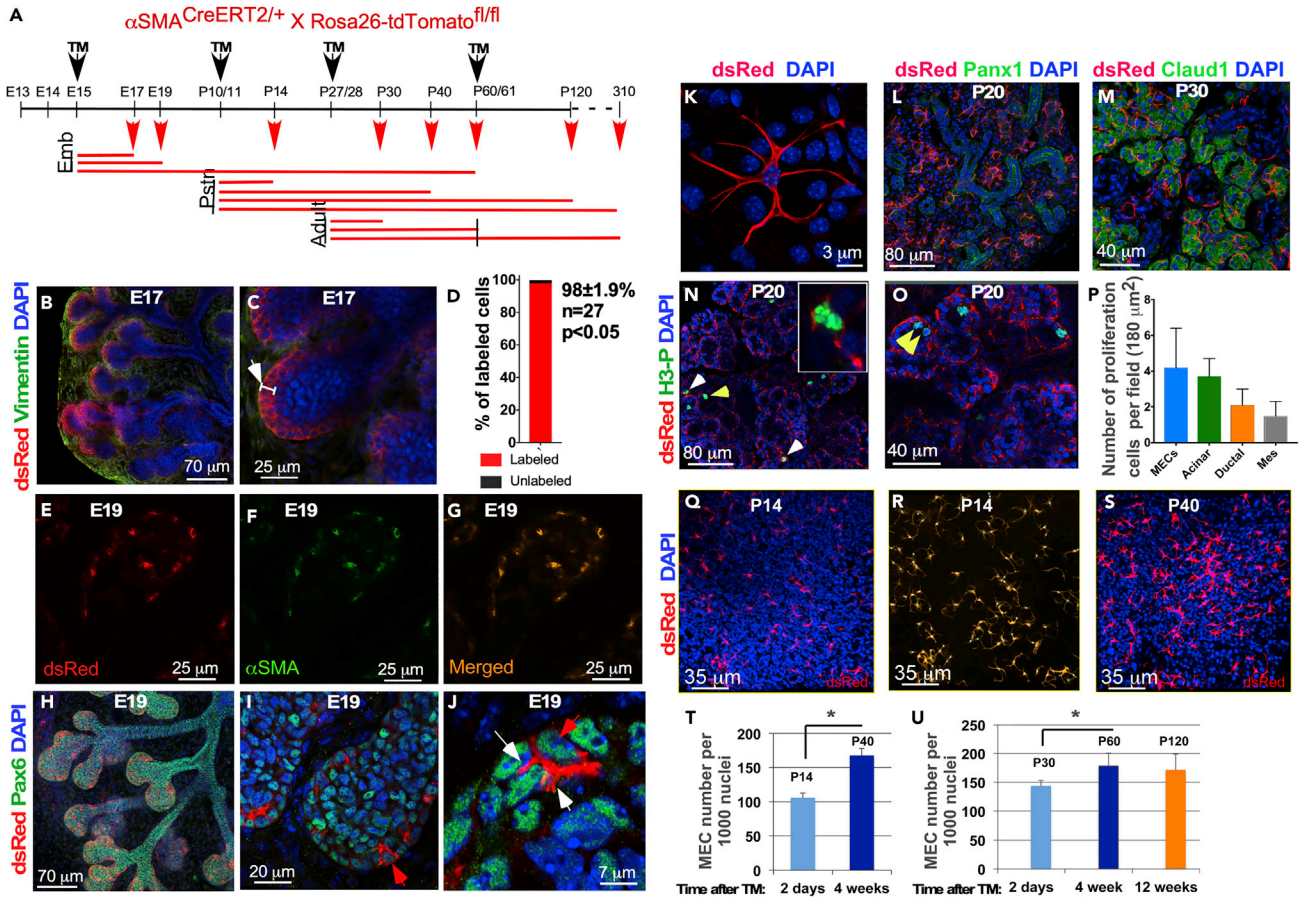

Figure 4. Analysis of MEC Lineage Using the *SMA^{CreERT2}:R26-tdTomato* Mouse

(A) Experimental design diagram. TM was administered during embryonic (E15) development, postnatal (P10/11) development, and adulthood (P27/28 and P60/61) and analyzed at variable times.

(B and C) Labeled MECs were found in the external layer of cells of the LG buds (white arrow in C). They did not have processes and presented epithelial morphology.

(D–G) (D) Labeling efficiency in the *SMA$^{CreERT2:}$R26-tdTomato* mice, as determined by co-immunostaining with the SMA antibody at E19 (E–G) (n = 27; $p < 0.05$, where n = number of glands).

(H–J) At E19 MECs still remain to be associated with distal parts of LG epithelial tree (H) and mainly found within the LG buds (I), where they form small processes (J; white arrows). All epithelial cells, including MECs, express Pax6 (green) (J, red arrow: Pax6-expressing MEC).

(K–M) (K) By P30 the labeled cells acquired a mature MEC phenotype, i.e., small cell body with several long processes. During postnatal development all MECs maintained close association with the maturating acinar component of the LG, as shown by immunostaining with the ductal marker Panx1 (L, green) and acinar marker Claudin 1 (M, green).

(N and O) MECs and other epithelial cells proliferate during postnatal development, as shown by immunostaining with the anti phospho-histone H3 antibody (green; proliferating MECs, yellow arrowheads; proliferating acinar cells, white arrowheads). Insert in (N) shows proliferating MEC at higher magnification. (O) shows two proliferating MECs (yellow arrowheads) in one acinus.

(P) Quantification of proliferating cells within different LG compartments (MEC, acinar, ductal, and mesenchymal [mes]). Results show mean ± SD, n = 56, * $p < 0.05$, two-tailed t test.

(Q–S) MECs were labeled at P10/11 and quantified at P14 (Q) and P40 (S); quantification was performed using IMARIS software. Example is shown in (R).

(T) Plot showing results of MEC quantification (n = 35, * $p < 0.05$, results show mean ± SD; two-tailed t test).

(U) Similarly, MECs were labeled at P27/28 and quantified at P60 and P120. Number of MECs in the LG significantly increases by P60 but remains almost unchanged between P60 and P120 (n = 28; *$p < 0.05$; results show mean ± SD; two-tailed t test).

Appearance of new unlabeled but SMA$^+$ MECs was especially obvious at the distal parts of the LG, where gland growth occurs in adult mice (compare central parts of the LG Figures 5D–5F and distal parts of the gland Figures 5G–5I). The increasing number of unlabeled αSMA$^+$/dsRed$^-$ MECs observed after longer chase periods suggest that MEC progenitors that are negative for αSMA expression may indeed be present in adult LG.

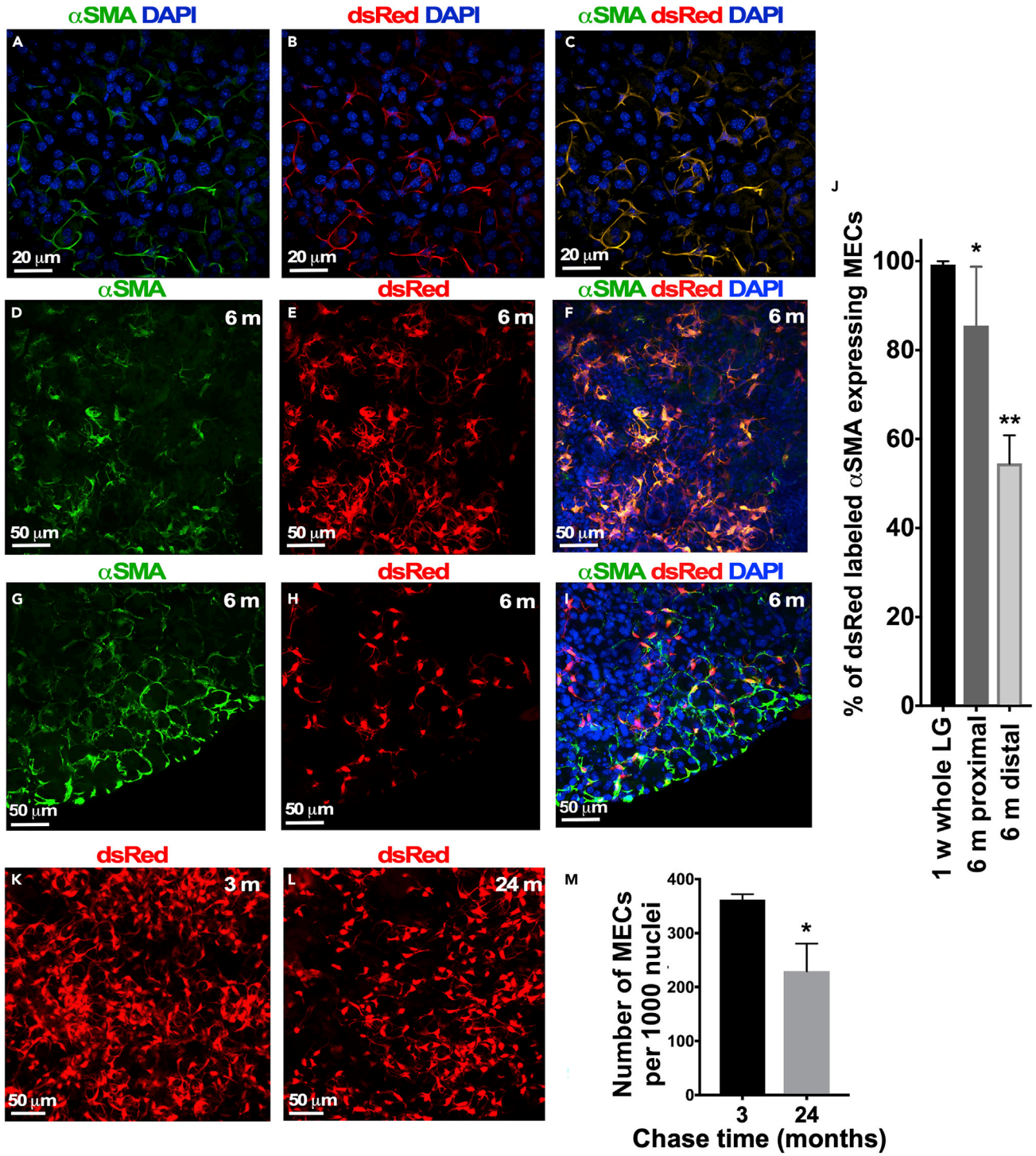

Figure 5. Analysis of MEC Lineage in Adult and Aged SMA$^{CreERT2/+}$:Rosa26-Tomato$^{fl/fl}$ Mice

(A–C) Co-immunostaining of MECs genetically labeled at P13/14 (red) with αSMA antibody (green) after 1 week of chase (P21). (A) Immunostaining with αSMA antibody. (B) Genetically labeled MECs. (C) Merged images.

(D–I) Co-immunostaining of MECs labeled at P14 (red) with αSMA antibody (green) after 6 months of chase (P200). (D–F) Most of MECs in the proximal (central) part of the LG also labeled with the αSMA^{+} antibody (green), whereas the distal part of the LG contains labeled (red) and unlabeled (green) MECs (G–I).

(J) Graphical representation of the results shown in (A–I). *n = 36; $p < 0.01$; **n = 28, $p < 0.01$, mean ± SD; two-tailed t test. Analysis of 14 LGs obtained from females, 7–12 sections per LG.

Figure 5. *Continued*

(K and L) Number of labeled MECs decreases with age. TM was administered at P13/14, and a number of MECs were analyzed at 3 (K) and 24 months (L). (M) Quantification of the labeled MECs in the LGs after 3 and 24 months of chase. The number of labeled MECs is significantly decreased in aged mice. *Analysis of 15 LG obtained from 4 females aged 3 months old and 5 females aged 24 months (105 sections); $p < 0.05$. Results show mean ± SD; two-tailed t test.

Next, we compared the number of labeled MEC cells between littermates labeled at P13/14 following 3 and 24 months after TM administration (Figures 5K and 5L). Quantification of labeled dsRed$^+$ cells in the LG showed significant decrease in number of labeled cells in old compared with young mice (Figure 5M). At the same time a substantial number of labeled MECs were still present even after a 24-month chase, again suggesting that MEC progenitors are long-lived cells. Labeled cells were found only in the MEC lineage, suggesting that in the LG αSMA$^+$ MEC lineage is a distinct cell lineage.

Lacrimal Gland SMA$^+$ MEC Can Contribute to Epithelial Regeneration following IL-1α Injury

Although we did not observe SMA$^+$ MECs giving rise to other epithelial cell types in the LG during development and homeostasis, we further challenged the system by injuring the gland with interleukin (IL)-1α administration. IL-1α injection induces a severe inflammatory response in the LG that leads to severe destruction of acinar cells in the injected LG lobules (Figure S7), followed by gland regeneration in 7–14 days (Zoukhri et al., 2008). To follow the MEC fate after injury we labeled MECs in the *SMA-CreERT2/+:R26-Tomato$^{fl/fl}$* mice at P28/30 (end of LG postnatal development, 6 mice, 2 experiments) or at P58/60 (adult LG, 12 mice, 4 experiments) by TM administration (Figure 6A), and 10 days later (at P40 or P75 correspondingly), the LG on one side of the animal was injected with saline (vehicle control) and the other was injured with IL-1α. Analysis of both the distribution and appearance of labeled cells was performed 2 weeks after injection (at P55 or P85) when LG regeneration is complete (Figure 8A). In control LGs (saline injected), all labeled cells had morphology and distribution characteristic of MECs and no other cell types were labeled (Figures 6B and 6C). In the glands injected with IL-1α, most labeled cells had MEC-like appearance; however, a small percent (9.8% ± 3.5% at P55 and 7.5% ± 4.4% at P85) of labeled acinar cells (i.e., of MEC origin) was found (Figures 6D–6F). These cells also highly expressed Panx1, which in the adult LG labels both acinar and ductal cells but has very low expression in MECs (Basova et al., 2017). Taken together, these data demonstrate that following injury at least some of the MECs were able to contribute to the repair of another epithelial component and retain some plasticity throughout the life of the organism.

Analysis of Runx1$^+$ Cell Lineage

We have previously demonstrated that the transcription factor Runx1 is expressed in the LG epithelium during development and marks ductal stem/progenitor cell compartments in the adult LG (Voronov et al., 2013). Using the TM-inducible *Runx1^{MerCreMer}:R26-Confetti$^{fl/+}$* mouse, we traced Runx1$^+$ lineage in the LG (Figure 7A). TM administration at E14-15 (one bud stage) revealed mosaic labeling of LG bud epithelium at E16-17 (Figures 7B and 7C). Next, we analyzed the population dynamics of Runx1-expressing cells after a longer chase period. Although the epithelial trees remained multicolored after a 5-week chase (at P30), discrete regions began to develop single-colored epithelial cell clones of all lineages (Figure 7D). Following a 9-week chase (at P60), large clones were detected in all LG compartments (ductal cells, acinar cells, and MEC) (Figures 7E–7G).

In contrast, TM administration to *Runx1^{MerCreMer}:R26-Confetti$^{fl/+}$* mice during late postnatal development (at P20/21) and analysis after 1.5 and 23 weeks of chase revealed labeling mostly within ducts (intercalated ducts and basal cells in inter- and intra-lobular ducts) with only a small proportion of cells labeled in the acinar cell compartment (Figures 7H–7K). These findings indicate that the lineage restriction of Runx1-expressing cells occurs rapidly after birth. Our data also suggest that during embryonic and maybe early postnatal development some epithelial progenitor cells are multipotent and can differentiate into several epithelial cell lineages; however, they become lineage-restricted during late postnatal development and in adulthood.

Expression Pattern of Stem/Progenitor Cell Markers in the Human LG

To determine the relevance of the data collated from our mouse models to humans, we analyzed the expression of several key transcription factors and other progenitor cell markers in human donor LGs.

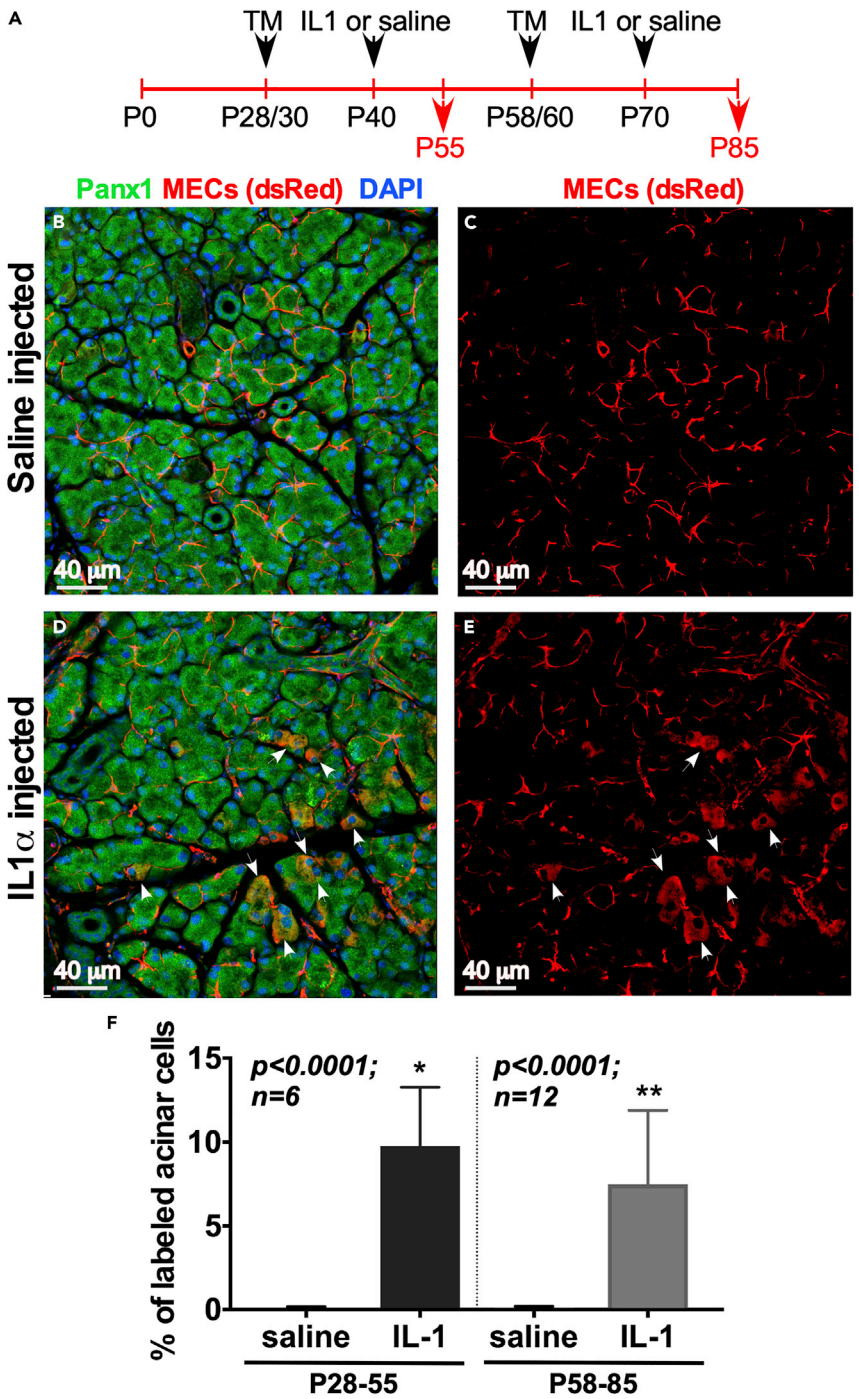

Figure 6. After LG Injury, MECs Repair the Acinar Epithelial Component

(A) Experimental design diagram. In the injury experiments we used females because dry eye disease is prevalent in females and LGs in females are smaller, ensuring a significant LG damage (also see Figure S7). The *SMA*^{CreERT2}*:Rosa26-tdTomato* female mice were injected with TM for three consecutive days (at P28–P30 or P58–P60) to label MECs, and 10 days later the LGs on one side of the animal were injured by IL-1α, whereas LGs on the other side of the animal were injected with saline (vehicle control). At least two to four independent experiments were performed at each stage. Mice were sacrificed 2 weeks later, and LGs were processed for frozen section preparation, immunostaining, and analysis: P28–P55: two independent experiments, 6 mice; 6 control and 6 IL-1α-injected LGs were studied; P58–P85: four independent experiments, 12 mice, 12 control and 12 IL-1α-injected LGs were analyzed.

Figure 6. *Continued*

(B–E) (B and C) In control (saline-injected) LG MECs retain an MEC phenotype and do not give rise to any other cell types, whereas after LG acute injury with IL-1α (D and E) a subset of MECs could acquire different fate and contribute to the acinar compartment of the LG.

(F) Cell quantification for each condition in each experiment (control or injured) was performed in sections (5 random sections per gland with 5–7 fields per section were analyzed).Total number of labeled cells in each gland were considered 100%; acinar cells were immunostained with the Panx1 antibody (acinar and ductal marker in adult mice) and percentage of labeled acinar cells has been determined. *P28–P55: two-tailed t test n = 6, $p < 0.001$ two-tailed t test; **P58–P85: n = 12, $p < 0.0001$, two-tailed t test. All results show mean ± SD. See also Figure S7.

Thus, Pax6, a known marker of self-renewing epithelial progenitors, analogous to the mouse, was localized to distal epithelial cells (Figure 8A). Krt5 and Krt14 protein expression was also found in the epithelial component of human LG (Figures 8B, 8C, and S8A–S8F). As shown by co-immunostaining with Krt14 (Figures S8A–S8C), Krt5 (Figures S8D–S8F), and αSMA antibody, high levels of Krt5 and Krt14 expression were found in the epithelial ducts and MECs, whereas Krt19, a marker of luminal ductal epithelia, was not expressed in the MEC (Figures S8G–S8I). Sox9 was expressed in the nuclei of epithelial component of the gland (Figures 8D and 8E), and Sox10 was found only in a subset of epithelial cells (Figure 8F). Similar to the mice (Gromova et al., 2017), human THBS1 was expressed in the MECs and ducts (Figure 8H). Control IgGs did not show any staining (Figure 8G). Thus, human LGs show a high level of similarity to the mouse with regard to expression patterns of putative stem/progenitor cell and basal cell markers.

DISCUSSION

In the current study, using cell lineage and LRC analysis we show the existence of a complex stem/progenitor cell hierarchy during LG development homeostasis and repair.

Herein, we demonstrated that during embryogenesis, the branching LG epithelium contains multipotent stem/progenitor cells able to give rise to several cell lineages (Figures 9A and S9A). Based on our previous studies these multipotent cells may express several stem/progenitor cell markers such as Sox9, Pax6, Runx1, c-kit, and Krt5/14 (Gromova et al., 2017; Voronov et al., 2013). Following birth, however, lineages become established and the fate of progenitor cell descendants becomes restricted (Figures 9B and S9B). This was exemplified by $Runx1^+$ embryonic progenitors that give rise to multiple cell lineages, whereas Runx1-expressing cells labeled in late postnatal development give rise mainly to the basal ductal cells. Moreover, Krt14-expressing cells labeled at early stages of postnatal development could be found in all lineages: MEC, basal ductal cells, and less frequently in acinar and luminal cells, whereas $Krt14^+$ cells labeled in adult LGs give rise to only MEC and basal ductal cells. Our recent data suggest that partial specification of distal and proximal parts of the LG buds occurs sometime in embryonic development (Thotakura et al., 2019) (Figure 9A). Farmer and coauthors (Farmer et al., 2017) suggest that ductal and acinar cells in the LG form unique populations by P4. In contrast, our current study and analysis of Sox10 mutant mouse (Chen et al., 2014) suggest that the establishment of distal (MEC and acinar) and proximal (ductal) cell lineages may happen much earlier during embryonic development (Figure 9A). Thus distal parts of the developing LG buds are exposed to the mesenchymally expressed fibroblast growth factor-10 (Fgf10) (Makarenkova et al., 2000, 2009) that most likely controls Sox10 expression (Chen et al., 2014) and the fate of acinar and MEC cells. Supporting this idea, our previous study showed that ectopic Fgf10 expression/application was able to induce an ectopic acinar cell formation in the cornea and conjunctiva (Govindarajan et al., 2000; Makarenkova et al., 2000). However, it is still possible that a small number of multipotent epithelial progenitor cells exist in the LG during postnatal development and early adulthood.

Our current results correlate with data from other exocrine glands showing that lineage-restricted stem/progenitor cells sustain the development, long-term maintenance, and regeneration of specific cell lineages (Aure et al., 2015; Emmerson and Knox, 2018; Van Keymeulen et al., 2017).

Thus, in our model LG multipotent stem/progenitor cells differentiate during embryonic development into proximal $Sox10^-$ and distal $Sox10^+$ cell lineages (Figure 9A), which are further restricted into $Sox10^-$ ductal (basal, luminal, and intercalated) and $Sox10^+$ lineages (acinar and MEC) during early postnatal development (Figure 9B). However, it is indeed possible that cells retain some plasticity during adult life and may be able to transdifferentiate following injury (Figure 9C; indicated by red arrow).

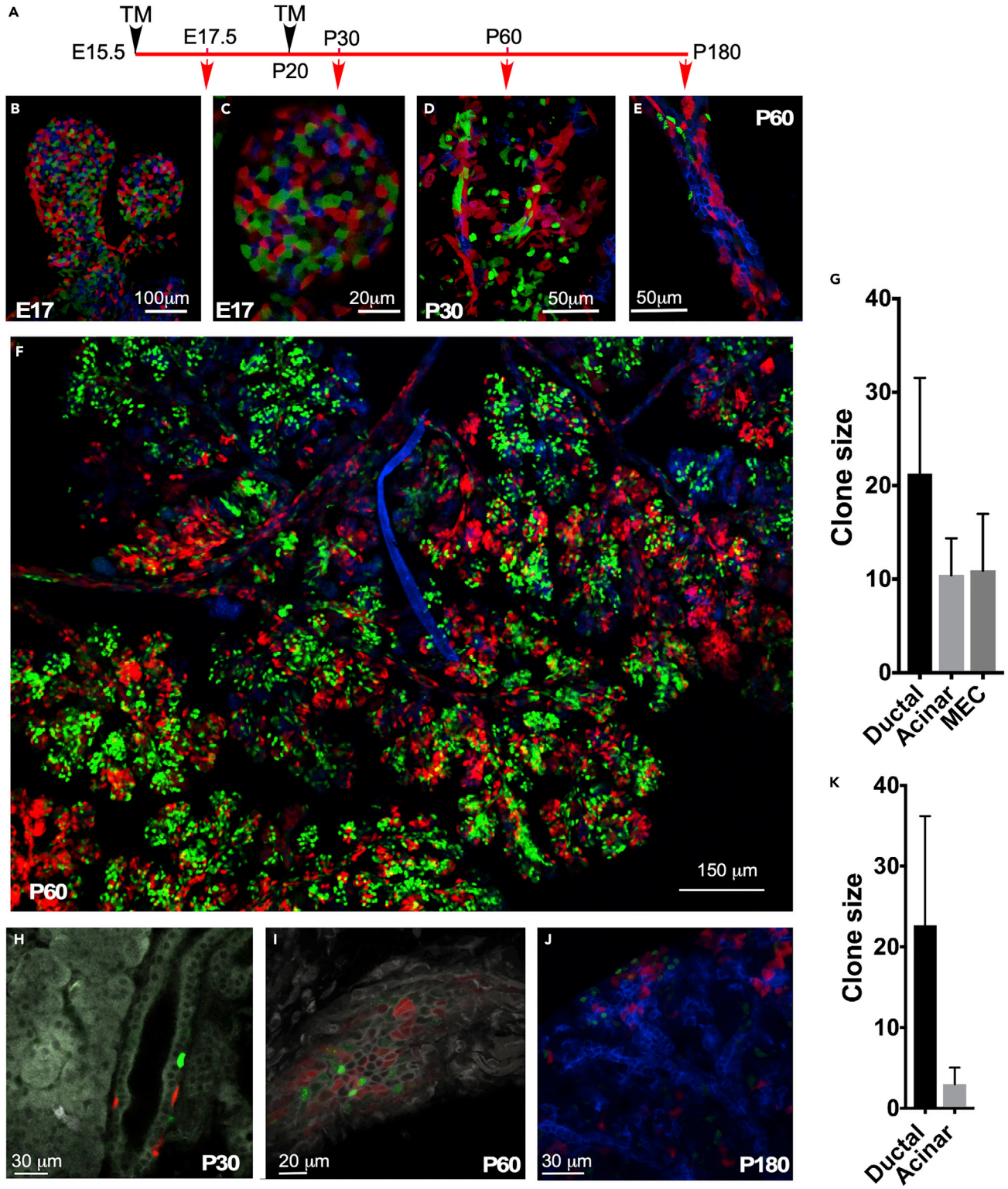

Figure 7. Runx1^{+} Embryonic Progenitors Give Rise to Multiple Cell Lineages, whereas Runx1-Expressing Cells in Late Postnatal Development Are Restricted to the Basal Ductal Cell Lineage

(A) The Runx1 $^{Mer-Cre-Mer/+}$:R26-Confetti$^{fl/+}$ mice were injected with tamoxifen (TM) at E15.5, and LGs were analyzed at E17, P30, P60, and P180. (B–F) (B and C) Mosaic labeling of epithelial cells at E17. At P30 (D) and P60 (E and F) cells labeled during embryogenesis form clones in all epithelial compartments of the LG.

Figure 7. *Continued*

(G) Quantification of clone sizes over time after TM administration during embryonic development (cells were labeled at E17 and quantified at P60). 16 mice (LG from 10 females obtained from 3 litters were analyzed). Clonal size is represented by the mean of number of cells per clone ± SD.

(H–J) TM administration during late postnatal development at P20 leads to labeling of cells mainly in basal ductal compartment. Only a few acinar cells were labeled.

(K) Quantification of clone sizes over time in adult LG (cells were labeled at P20 and quantified at P180). Clonal size is represented by the mean of number of cells per clone ± SD.

Intriguingly, we found that LG SMA$^+$ MEC lineage is established early in embryonic development (Figures 4B, 4C, and 9A) and, similar to other glands (Anderson et al., 2017), originates from the external layer of cells within the distal bud and participates in postnatal LG growth expansion. These embryonic long-lived SMA$^+$ MECs do not differentiate into cells of other lineages under homeostatic conditions. Moreover, analysis of SMA$^+$ MEC clonal expansion in *SMA^{CreERT2}:R26-Confetti* mice suggests the existence of two subpopulations of cells during postnatal development short-term and long-term MECs.

It has been previously suggested that the SMA$^+$ MEC cell linage in adult LGs may contain multipotent SCs (Shatos et al., 2012, 2016). Furthermore, our group has observed a high degree of plasticity in both epithelial cells (Gromova et al., 2017) and MECs *in vitro*; however, the current investigation did not provide supporting evidence that this occurs *in vivo* under homeostatic conditions (Figures 3 and 4). Taken together with the observation that slow proliferating LRCs are not found in the MEC lineage following an 8-week chase period, it implies that the SMA$^+$ MEC lineage in the LG is a distinct lineage that is maintained by proliferating lineage-restricted SMA$^+$ progenitors originating from the distal layer of the epithelia within the LG bud during embryonic development. These SMA$^+$ progenitors proliferate and differentiate during postnatal development in close association with LG acinar cells (Basova et al., 2017; Farmer et al., 2017; Makarenkova and Dartt, 2015). Embryonic (Chen et al., 2014; Garg and Zhang, 2017) and adult (Figures S1I–S1K) acinar cells and MECs continue to express Sox10 in both the mouse and human (Figure 8F) LGs. Moreover, Sox10 knockout mice lose most of their acinar cells and all acini-associated MECs (Chen et al., 2014). These findings support our proposition that the majority of acinar cells and MECs in the adult LG are direct descendants of a common Sox10$^+$ acinar/MEC embryonic progenitor cell (Figure 9A). If development and differentiation of these common progenitors is perturbed during LG morphogenesis, other SCs/progenitor cells cannot completely replace lost cells from these compartments because the period of LG active expansion has already been completed.

Our label retention study using intrinsic genetic marking of LRCs showed the existence of slow-cycling stem/progenitor cells in the basal layer of the excretory ducts and in the intercalated ducts, further suggesting the existence of reserve cells in the LG. Whether common multipotent progenitors exist in adult LG still needs to be determined, as unique markers for this progenitor population are currently unknown. However, an increasing number of unlabeled MECs observed after longer chase periods of SMA$^+$ MEC lineage suggests that MEC progenitors that are negative for αSMA expression may indeed be present in adult LG. At the same time our results also indicate that the majority of MECs in the LG are maintained by lineage-restricted SMA$^+$ progenitors that exclusively contribute to the fast growth/expansion of the MEC lineage during postnatal development, whereas slow growth of adult homeostatic LG could be supported by both lineage-restricted SMA$^+$ MEC progenitors and SMA$^-$ common acinar/MEC cell progenitors. However, differentiated MECs retain some proliferative potential in adult uninjured LG (Burgess et al., 1996; Shatos et al., 2012) and show a rapid proliferative response following gland injury (Burgess et al., 1996). We showed that SMA$^+$ MECs retained plasticity *in vivo* and can differentiate into acinar cells after acute LG injury (Figure 9C). MEC plasticity has been reported in other glandular organs, such as mammary and submucosal glands, where they function as a reserve of stem/progenitor cells to regenerate tissue upon injury (Lynch et al., 2018; Prater et al., 2014; Tata et al., 2018). It is likely that in the LG, MECs perform a similar function, suggesting that in glandular organs, injury reveals the plasticity of unipotent progenitors and possibly differentiated MEC cells. Taken together our findings further support a model of lineage restriction of embryonic stem/progenitor cells in the early postnatal LGs and highlight extensive heterogeneity and selected redundancy within the adult LG progenitor cell pool. Similar findings were observed in the mammary gland (another exocrine gland) by molecular profiling and single-cell RNA sequencing, demonstrating that multipotent embryonic progenitor cells express a unique hybrid (basal and luminal) signature associated with different lineages (Wuidart et al., 2018). Thus, our results and other publications support the notion that a developmental "switch" exists that restricts the multipotent activity of progenitor cells to unipotency or bipotency in various glandular

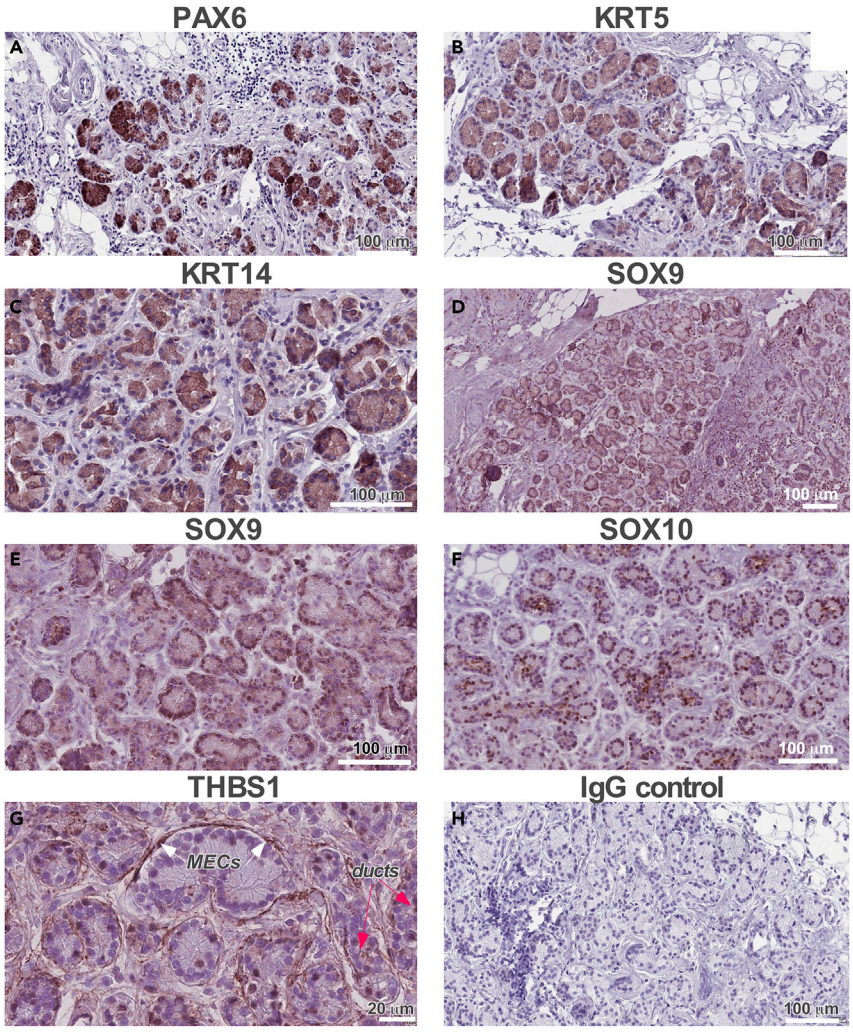

Figure 8. Expression of the Progenitor Cell Transcription Factors and Basal Cell Markers in Adult Human LGs

(A–F) Similar to mouse LGs (Makarenkova et al., 2000), PAX6 (A) is expressed in the distal epithelial structures, whereas KRT5 (B) and KRT14 (C) are expressed in ductal epithelial derivates. SOX9 (D and E) is found in the nuclei of LG epithelium, whereas SOX10 (F) is restricted to the nuclei of acinar cells.

(G) THBS1 is expressed in MECs (MECs, white arrows) and ducts (ducts, red arrows).

(H) Negative control: section was treated with nonspecific IgG. Human LGs from three female donors (ages at the time of death were 62, 84, and 90 years) were obtained from Advanced Tissue Services (Phoenix, AZ, USA).

See also Figure S8.

tissues. However, the mechanism that controls the process of lineage restriction still needs to be elucidated.

Our Krt14 lineage data show the presence of another specialized basal ductal cell lineage (Figure 9C). One function of the multilayered excretory inter- and intra-lobular ducts in LGs is to maintain fluid propagation and to drain individual acini and lobes to maintain tear flow to the ocular surface. We found that a large subset of Krt14^{+} basal ductal cells continue to proliferate and differentiate into contractile basal ductal cells that possess small cell processes and contain filamentous actin (F-actin). The contractile function of basal ductal cells was reported by other investigators who showed tonofilaments within basal cells of LG ducts (Iwamoto and Jakobiec, 1982). Thus, in adult LGs, the Krt14 cell lineage appears to be restricted to two contractile cells types, namely, MECs and basal ductal cells, which facilitate the release and circulation of the watery tears.

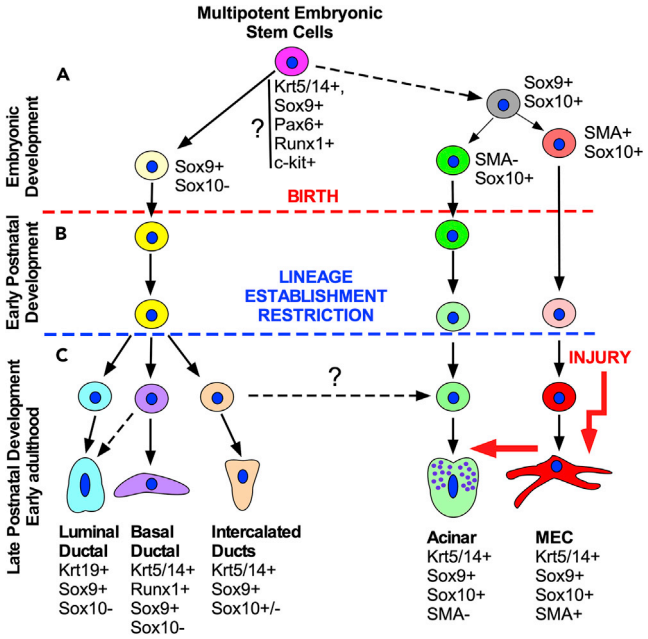

Figure 9. Schematic Representation of the LG Lineage

Multipotent LG progenitor/stem cells exist in the embryonic LG and early postnatal development and give rise to all cell lineages.

(A) Multipotent LG progenitor/stem cells co-express common markers identified early in LG development. The Sox10-negative cells give rise to ductal lineages, whereas Sox10-positive progenitor give rise to acinar and MEC lineages.

(B and C) (B) Embryonic LG progenitor cells become predisposed toward one lineage as development proceeds and adopt specific marker profiles and location within the epithelium. This lineage restriction may happen at different time in each lineage. For example, MEC lineage is established very early during embryonic development (A), whereas ductal cell lineage is established later during postnatal development. At the same time unipotent MECs in postnatal and adult LGs have certain level of plasticity and may undergo *in vivo* reprogramming induced by LG injury (C). Thus, the MECs may have reserved MEC progenitors able to help with LG repair after injury (red arrow). (C) It is possible that common progenitor of MEC and acinar lineages is localized in the intercalated ducts (dashed arrow). Solid arrows, reported connections; dashed arrows, possible connections.

See also Figure S9.

The longevity of the unipotent cells such as MECs and basal ductal progenitors, and their ability to participate in tissue regeneration, suggest the universal plasticity of these and possibly other cell types in the LG. The labeling patterns and analysis of injured LG suggest a model where injury/acute inflammation activates proliferation of the existing lineage-restricted progenitors, followed by the reserve progenitor cells and their progenies.

Comparison of stem/progenitor cell and basal markers in mouse and human LGs revealed a high level of similarity in their expression patterns. For example, as an important regulator of mouse LG development (Chen et al., 2014) Sox9 labels all ductal cells and MECs, whereas Sox10 expression remains to be restricted to acinar cells and MECs. Similar patterns of Sox9 and Sox10 expression were found in human LGs (Figures 8D–8F). These findings suggest that the mouse and human LG may have similar mechanisms that control stem and progenitor cell function. Further analysis of mouse and human LGs would help to delineate the mechanism by which the progenitor cell pool is established and functions. This of course has far-reaching clinical implications. Recently, SC transplantation therapy has emerged as a promising method to treat both LGs and salivary gland disorders (Emmerson and Knox, 2018; Feng et al., 2009; Gromova et al., 2017). We and others have demonstrated that transplantation of putative epithelial progenitor cells isolated from "healthy" mouse LG or submandibular gland can restore function of the diseased organs, suggesting that stem/progenitor cells have a therapeutic role in ADDE (Feng et al., 2009; Gromova et al., 2017). However, efficiency of different types of stem/progenitor and different transplantation strategies remain to be resolved before successful clinical applications of the cell-based therapies are introduced to treat diseases that affect lacrimal and salivary glands.

In summary, LG lineage tracing has highlighted the existence of long-lived lineage-restricted unipotent and multipotent reserve cells that drive morphogenesis, homeostasis, and repair of the LG epithelial tree. Our findings provide important new details about glandular SC biology and reveal fundamental similarities and differences in the homeostatic and regenerative potential of stem and progenitor cells between LG and other glandular tissues.

Limitations of the Study

Our genetic lineage-tracing studies in the mouse LG using K14, Runx1, and SMA (Acta2) drivers achieved *in vivo* permanent marking of specific populations of cells at specific stages of LG morphogenesis. Although analysis of these targeted cell populations provided us with valuable information on the LG epithelial differentiation hierarchy, these models have relied on prior assumptions regarding the specificity and consistency of the expression of the chosen gene promoters.

Resource Availability

Lead Contact

Further information and requests for resources and reagents should be directed to and will be fulfilled by the Lead Contact, Helen P. Makarenkova (hmakarenk@scripps.edu).

Materials Availability

Mouse lines generated in this study by breeding are available from the Lead Contact with a completed Materials Transfer Agreement.

Data and Code Availability

This study did not generate/analyze [datasets/code].

METHODS

All methods can be found in the accompanying Transparent Methods supplemental file.

SUPPLEMENTAL INFORMATION

Supplemental Information can be found online at https://doi.org/10.1016/j.isci.2020.101230.

ACKNOWLEDGMENTS

This study is supported by National Institutes of Health (NIH), National Eye Institute (NEI), United States, Grants 5R01EY026202 and 5R01EY028983 to H.P.M. and 5R01EY021510 to J.V.J.; by National Institute of Arthritis and Musculoskeletal and Skin Diseases (NIAMS), United States, Grant AR055607 to I.K.; by a Ser Cymru/Marie-Sklodowska Curie Fellowship from the Welsh Government and the European Horizon 2020 program to G.J.P.; and by grants APP1101078 and APP1156944 from the National Health and Medical Research Council, Australia to N.D.G.

AUTHOR CONTRIBUTIONS

Conceptualization, H.P.M., J.V.J., and G.J.P.; Methodology, H.P.M., A.R., J.V.J., and G.J.P.; Investigation, L.B., V.D., G.J.P., A.R., and T.U.; Validation, H.P.M., A.R., I.K., and G.J.P.; Formal Analysis, L.B., A.R., G.J.P., and H.P.M.; Writing – Original Draft, H.P.M and G.J.P.; Writing –Review & Editing, H.P.M., J.V.J., G.J.P., A.R., N.D.G., L.B., D.T.T., and I.K.; Funding Acquisition, H.P.M., J.V.J., N.D.G. I.K., and G.J.P.; Resources, I.K., D.T.T., and D.P.; Supervision, H.P.M., N.D.G., J.V.J., and G.J.P.

DECLARATION OF INTERESTS

The authors declare no competing interests.

Received: December 4, 2019
Revised: April 3, 2020
Accepted: May 29, 2020
Published: June 26, 2020

REFERENCES

Abe, J., Sugita, A., Hamasaki, M., Nakamura, K., Iwanaga, S., Nagae, K., Atsuji, K., Tsunawaki, A., Abe, T., Matsumoto, T., et al. (1981). Scanning electron microscopic observations of the myoepithelial cells of normal and contracting status in the rat harderian gland. Kurume Med. J. *28*, 103–112.

Anderson, P.J., Lynch, T.J., and Engelhardt, J.F. (2017). Multipotent myoepithelial progenitor cells are born early during airway submucosal gland development. Am. J. Respir. Cell Mol. Biol. *56*, 716–726.

Aure, M.H., Konieczny, S.F., and Ovitt, C.E. (2015). Salivary gland homeostasis is maintained through acinar cell self-duplication. Dev. Cell *33*, 231–237.

Avci, A., Gunhan, O., Cakalagaoglu, F., Gunal, A., and Celasun, B. (2012). The cell with a thousand faces: detection of myoepithelial cells and their contributions in the cytological diagnosis of salivary gland tumors. Diagn. Cytopathol. *40*, 220–227.

Basova, L.V., Tang, X., Umasume, T., Gromova, A., Zyrianova, T., Shmushkovich, T., Wolfson, A., Hawley, D., Zoukhri, D., Shestopalov, V.I., et al. (2017). Manipulation of Panx1 activity increases the engraftment of transplanted lacrimal gland epithelial progenitor cells. Invest Ophthalmol. Vis. Sci. *58*, 5654–5665.

Burgess, K.L., Dardick, I., Cummins, M.M., Burford-Mason, A.P., Bassett, R., and Brown, D.H. (1996). Myoepithelial cells actively proliferate during atrophy of rat parotid gland. Oral Surg. Oral Med. Oral Pathol. Oral Radiol. Endod. *82*, 674–680.

Chen, Z., Huang, J., Liu, Y., Dattilo, L.K., Huh, S.H., Ornitz, D., and Beebe, D.C. (2014). FGF signaling activates a Sox9-Sox10 pathway for the formation and branching morphogenesis of mouse ocular glands. Development *141*, 2691–2701.

Chibly, A.M., Querin, L., Harris, Z., and Limesand, K.H. (2014). Label-retaining cells in the adult murine salivary glands possess characteristics of adult progenitor cells. PLoS One *9*, e107893.

Dartt, D.A. (2009). Neural regulation of lacrimal gland secretory processes: relevance in dry eye diseases. Prog. Retin. Eye Res. *28*, 155–177.

Emmerson, E., and Knox, S.M. (2018). Salivary gland stem cells: a review of development, regeneration and cancer. Genesis *56*, e23211.

Faraldo, M.M., Teuliere, J., Deugnier, M.A., Taddei-De La Hosseraye, I., Thiery, J.P., and Glukhova, M.A. (2005). Myoepithelial cells in the control of mammary development and tumorigenesis: data from genetically modified mice. J. Mammary Gland Biol. Neoplasia *10*, 211–219.

Farmer, D.T., Nathan, S., Finley, J.K., Shengyang Yu, K., Emmerson, E., Byrnes, L.E., Sneddon, J.B., McManus, M.T., Tward, A.D., and Knox, S.M. (2017). Defining epithelial cell dynamics and lineage relationships in the developing lacrimal gland. Development *144*, 2517–2528.

Feng, J., van der Zwaag, M., Stokman, M.A., van Os, R., and Coppes, R.P. (2009). Isolation and characterization of human salivary gland cells for stem cell transplantation to reduce radiation-induced hyposalivation. Radiother. Oncol. *92*, 466–471.

Garg, A., and Zhang, X. (2017). Lacrimal gland development: from signaling interactions to regenerative medicine. Dev. Dyn. *246*, 970–980.

Govindarajan, V., Ito, M., Makarenkova, H.P., Lang, R.A., and Overbeek, P.A. (2000). Endogenous and ectopic gland induction by FGF-10. Dev. Biol. *225*, 188–200.

Gromova, A., Voronov, D.A., Yoshida, M., Thotakura, S., Meech, R., Dartt, D.A., and Makarenkova, H.P. (2017). Lacrimal gland repair using progenitor cells. Stem Cells Transl. Med. *6*, 88–98.

Gudjonsson, T., Adriance, M.C., Sternlicht, M.D., Petersen, O.W., and Bissell, M.J. (2005). Myoepithelial cells: their origin and function in breast morphogenesis and neoplasia. J. Mammary Gland Biol. Neoplasia *10*, 261–272.

Hamano, T. (2002). Atelocollagen punctal occlusion for the treatment of the dry eye. Adv. Exp. Med. Biol. *506*, 1283–1284.

Hawley, D., Tang, X., Zyrianova, T., Shah, M., Janga, S., Letourneau, A., Schicht, M., Paulsen, F., Hamm-Alvarez, S., Makarenkova, H.P., et al. (2018). Myoepithelial cell-driven acini contraction in response to oxytocin receptor stimulation is impaired in lacrimal glands of Sjogren's syndrome animal models. Sci. Rep. *8*, 9919.

Hirayama, M., Ogawa, M., Oshima, M., Sekine, Y., Ishida, K., Yamashita, K., Ikeda, K., Shimmura, S., Kawakita, T., Tsubota, K., et al. (2013). Functional lacrimal gland regeneration by transplantation of a bioengineered organ germ. Nat. Commun. *4*, 2497.

Iwamoto, T., and Jakobiec, F.A. (1982). A comparative ultrastructural study of the normal lacrimal gland and its epithelial tumors. Hum. Pathol. *13*, 236–262.

Khanal, S., Tomlinson, A., and Diaper, C.J. (2009). Tear physiology of aqueous deficiency and evaporative dry eye. Optom. Vis. Sci. *86*, 1235–1240.

Kuony, A., and Michon, F. (2017). Epithelial markers aSMA, Krt14, and Krt19 unveil elements of murine lacrimal gland morphogenesis and maturation. Front. Physiol. *8*, 739.

Leung, Y., Kandyba, E., Chen, Y.B., Ruffins, S., and Kobielak, K. (2013). Label retaining cells (LRCs) with myoepithelial characteristic from the proximal acinar region define stem cells in the sweat gland. PLoS One *8*, e74174.

Lynch, T.J., Anderson, P.J., Rotti, P.G., Tyler, S.R., Crooke, A.K., Choi, S.H., Montoro, D.T., Silverman, C.L., Shahin, W., Zhao, R., et al. (2018). Submucosal gland myoepithelial cells are reserve stem cells that can regenerate mouse Tracheal epithelium. Cell Stem Cell *22*, 779.

Makarenkova, H.P., and Dartt, D.A. (2015). Myoepithelial cells: their origin and function in lacrimal gland morphogenesis, homeostasis, and repair. Curr. Mol. Biol. Rep. *1*, 115–123.

Makarenkova, H.P., Hoffman, M.P., Beenken, A., Eliseenkova, A.V., Meech, R., Tsau, C., Patel, V.N., Lang, R.A., and Mohammadi, M. (2009). Differential interactions of FGFs with heparan sulfate control gradient formation and branching morphogenesis. Sci. Signal. *2*, ra55.

Makarenkova, H.P., Ito, M., Govindarajan, V., Faber, S.C., Sun, L., McMahon, G., Overbeek, P.A., and Lang, R.A. (2000). FGF10 is an inducer and Pax6 a competence factor for lacrimal gland development. Development *127*, 2563–2572.

Parfitt, G.J., Kavianpour, B., Wu, K.L., Xie, Y., Brown, D.J., and Jester, J.V. (2015). Immunofluorescence tomography of mouse ocular surface epithelial stem cells and their niche microenvironment. Invest Ophthalmol. Vis. Sci. *56*, 7338–7344.

Prater, M.D., Petit, V., Alasdair Russell, I., Giraddi, R.R., Shehata, M., Menon, S., Schulte, R., Kalajzic, I., Rath, N., Olson, M.F., et al. (2014). Mammary stem cells have myoepithelial cell properties. Nat. Cell Biol. *16*, 942–950, 941-7.

Raubenheimer, E.J. (1987). The myoepithelial cell: embryology, function, and proliferative aspects. Crit. Rev. Clin. Lab Sci. *25*, 161–193.

Rios, A.C., Fu, N.Y., Lindeman, G.J., and Visvader, J.E. (2014). In situ identification of bipotent stem cells in the mammary gland. Nature *506*, 322–327.

Roberts, C.W., Carniglia, P.E., and Brazzo, B.G. (2007). Comparison of topical cyclosporine, punctal occlusion, and a combination for the treatment of dry eye. Cornea *26*, 805–809.

Rouen, P.A., and White, M.L. (2018). Dry eye disease: prevalence, assessment, and management. Home Healthc. Now *36*, 74–83.

Schon, M., Benwood, J., O'Connell-Willstaedt, T., and Rheinwald, J.G. (1999). Human sweat gland myoepithelial cells express a unique set of cytokeratins and reveal the potential for alternative epithelial and mesenchymal differentiation states in culture. J. Cell Sci. *112* (Pt 12), 1925–1936.

Shackleton, M., Vaillant, F., Simpson, K.J., Stingl, J., Smyth, G.K., Asselin-Labat, M.L., Wu, L., Lindeman, G.J., and Visvader, J.E. (2006). Generation of a functional mammary gland from a single stem cell. Nature *439*, 84–88.

Shatos, M.A., Haugaard-Kedstrom, L., Hodges, R.R., and Dartt, D.A. (2012). Isolation and characterization of progenitor cells in uninjured, adult rat lacrimal gland. Invest Ophthalmol. Vis. Sci. *53*, 2749–2759.

Shatos, M.A., Hodges, R.R., Morinaga, M., McNay, D.E., Islam, R., Bhattacharya, S., Li, D., Turpie, B., Makarenkova, H.P., Masli, S., et al. (2016). Alteration in cellular turnover and progenitor cell population in lacrimal glands from thrombospondin 1(-/-) mice, a model of dry eye. Exp. Eye Res. *153*, 27–41.

Tan, X., Chen, Y., Foulsham, W., Amouzegar, A., Inomata, T., Liu, Y., Chauhan, S.K., and Dana, R. (2018). The immunoregulatory role of corneal epithelium-derived thrombospondin-1 in dry eye disease. Ocul. Surf. *16*, 470–477.

Tata, A., Kobayashi, Y., Chow, R.D., Tran, J., Desai, A., Massri, A.J., McCord, T.J., Gunn, M.D., and Tata, P.R. (2018). Myoepithelial cells of submucosal glands can function as reserve stem cells to regenerate airways after injury. Cell Stem Cell *22*, 668–683.e6.

Thotakura, S., Basova, L., and Makarenkova, H.P. (2019). FGF gradient controls boundary position between proliferating and differentiating cells and regulates lacrimal gland growth dynamics. Front. Genet. *10*, 362.

Van Keymeulen, A., Fioramonti, M., Centonze, A., Bouvencourt, G., Achouri, Y., and Blanpain, C. (2017). Lineage-restricted mammary stem cells sustain the development, homeostasis, and regeneration of the estrogen receptor positive lineage. Cell Rep. *20*, 1525–1532.

Visvader, J.E., and Stingl, J. (2014). Mammary stem cells and the differentiation hierarchy: current status and perspectives. Genes Dev. *28*, 1143–1158.

Voronov, D., Gromova, A., Liu, D., Zoukhri, D., Medvinsky, A., Meech, R., and Makarenkova, H.P. (2013). Transcription factors Runx1 to 3 are expressed in the lacrimal gland epithelium and are involved in regulation of gland morphogenesis and regeneration. Invest Ophthalmol. Vis. Sci. *54*, 3115–3125.

Wang, Y.L., Tan, Y., Satoh, Y., and Ono, K. (1995). Morphological changes of myoepithelial cells of mouse lacrimal glands during postnatal development. Histol. Histopathol. *10*, 821–827.

Wuidart, A., Ousset, M., Rulands, S., Simons, B.D., Van Keymeulen, A., and Blanpain, C. (2016). Quantitative lineage tracing strategies to resolve multipotency in tissue-specific stem cells. Genes Dev. *30*, 1261–1277.

Wuidart, A., Sifrim, A., Fioramonti, M., Matsumura, S., Brisebarre, A., Brown, D., Centonze, A., Dannau, A., Dubois, C., Van Keymeulen, A., et al. (2018). Early lineage segregation of multipotent embryonic mammary gland progenitors. Nat. Cell Biol *20*, 666–676.

You, S., Tariq, A., Kublin, C.L., and Zoukhri, D. (2011). Detection of BrdU-label retaining cells in the lacrimal gland: implications for tissue repair. Cell Tissue Res. *346*, 317–326.

Zhang, H., Boddupally, K., Kandyba, E., Kobielak, K., Chen, Y., Zu, S., Krishnan, R., Sinha, U., and Kobielak, A. (2014). Defining the localization and molecular characteristic of minor salivary gland label-retaining cells. Stem Cells *32*, 2267–2277.

Zhao, J., Mo, V., and Nagasaki, T. (2009). Distribution of label-retaining cells in the limbal epithelium of a mouse eye. J. Histochem. Cytochem. *57*, 177–185.

Zouchri, D., and Makarenkova, H.P. (2015). Role of stem cells in lacrimal and meibomian gland development and regeneration. In Stem Cells in Opthalmology, D.H. Scorsetti, V.L. Perez, and J.A.P. Gomes, eds. (Jaypee-Highlights Medical Publishers), pp. 165–178.

Zoukhri, D. (2006). Effect of inflammation on lacrimal gland function. Exp. Eye Res. *82*, 885–898.

Zoukhri, D., Fix, A., Alroy, J., and Kublin, C.L. (2008). Mechanisms of murine lacrimal gland repair after experimentally induced inflammation. Invest Ophthalmol. Vis. Sci. *49*, 4399–4406.

iScience, Volume *23*

Supplemental Information

Origin and Lineage Plasticity of Endogenous Lacrimal Gland Epithelial Stem/Progenitor Cells

Liana Basova, Geraint J. Parfitt, Alex Richardson, Vanessa Delcroix, Takeshi Umazume, Daniel Pelaez, David T. Tse, Ivo Kalajzic, Nick Di Girolamo, James V. Jester, and Helen P. Makarenkova

SUPPLEMENTAL INFORMATION

SUPPLEMENTAL FIGURES

Figure S1. *Analysis of GFP expression in the LG of unchased and chased H2B-GFP/K5tTA and mice. Related to figure 1.* (A-E') H2B-GFP/K5tTA mice were pulsed from P0 to P28 to label all cytokeratin 5^+ epithelial cells with nuclear green fluorescence protein (GFP). At P28, H2B-GFP/K5tTA mice were sacrificed and the LGs or frozen sections of glands were immunostained with anti-αSMA and analyzed for GFP expression. (A, C) Almost all MECs exhibited nuclear GFP; however, we also identified a small percentage of unlabeled MECs (B, white arrows). (C) Almost all cells of intercalated ducts labeled with GFP. (D) Example of excretory ducts in unchased LGs showing labeling in basal ductal cells (*BD* - white arrows). αSMA staining (red) detects pericytes in the blood vessels (D, red arrows). (E) Quantification of GFP expressing cells in different LG compartments. Approximately 35 randomly taken sections of approximately 10 mm length and 6 mm width and 5-7 fields of each section have been analyzed (MEC - myoepithelial cells, BD -basal ductal cells, ID – intercalated duct cells, LUM – luminal ductal cells, AC acinar cells). (E') An example of excretory duct (*ED*) image, showing a couple of labeled luminal cells (white arrows). This particular image was equalized using Photoshop, which allows to see the ductal cell shape. Note: Only a low percentage of labeled luminal cells were detected. (F-H) The H2B-GFP/K5tTA mice were pulsed from P0 to P28 to label proliferating cells. At P28, H2B-GFP/K5tTA mice were fed a doxycycline-containing diet for 8 weeks (chase) and frozen sections of the LGs obtained from these mice were immunostained with the Krt5 (F) or Krt14 (G and H, grey) and αSMA (G, red) to visualize basal ductal cells and MECs. No GFP was found in the acinar and luminal compartments. LRCs (green) are found in a subset of basal ductal cells expressing Krt5/Krt14 but not in MECs (G, *MEC*, red arrows). (I -K) Distal embryonic LG bud marker Sox10 (Chen et al., 2014) continues to be expressed in the distal epithelial structures (acinar and MEC cells) of the LG during early postnatal development (I and J) and adulthood (K, MECs - white arrows), but not in the ducts (*duct*).

Fifure S2. *Single channel images of Figure 1E. Related to Figure 1E.* (E') – DAPI; (E'') - GFP (LRCs). (E''') – Immunostaining for αSMA, (E'''') – immunostaining for c-kit.

Figure S3. *Single channel images of Figure 1F. Related to Figure 1F.* (F') – DAPI; (F'') - GFP (LRCs). (F''') – Immunostaining for αSMA, (F'''') – immunostaining for Krt14.

Figure S4 *Expression pattern of Krt5 and 14 in the LG. Related to Figure 2.* (A-D) Section of LG stained with Krt15 (green) Krt5 (pink) and αSMA (red) antibodies. (E-H) Immunostatining of LG lobule with Krt14 (red) and Krt5 (green) antibodies. Note: no acinar cells are labeled. (I-L) immunostaining of the LG at E19.5 with Krt14 (green) and Krt5 (red antibodies) showing labeling of basal layer of ducts. Nuclei labeled with DAPI. Although expression pattern of Krt5 and Krt14 was not completely overlapped (especially in MECs: (A, B, D and E-H) both keratins were found only within two compartments of the LG: MEC and basal ductal.

Figure S5. *Single channel images and DAPI of Figure 2C. Related to Figure 2C.* (C') Krt14 (dsRed) + DAPI; (C'') – Krt14 (GFP) +DAPI; (C''') - Immunostaining for αSMA (Orange) + DAPI, (C'''') – merged image. Scale bar is 8 μm.

Figure S6. *Apical parts of luminal cells and basal ductal cells show a high level of filamentous actin. Related to Figure 2.* (A, B) Rhodamine-phalloidin staining reveals filamentous actin in the apical part (*ap*) of the luminal ductal cells and in a subset of basal ductal cells (white arrows).

Figure S7. *IL1α injection induces severe damage of the LG acinar compartment. Related to Figure 6.* (A, B) LG structure 1 day after IL1α injection. Majority of acinar cells in IL1α injected LG lobules are destroyed. Acini left after IL1α injection are labeled by black arrows. Some acinar cells become dense, thus suggesting degeneration (red arrows). (C, D) LG structure 3 days after injury. Number of infiltrating cells decreases, and small regenerating acini appear (D, white arrowheads). (E) Control LG injected with vehicle (saline) (one day after injection) has normal structure. Paraffin sections of IL1α and saline injected LGs were stained with fast red. LGs were obtained from female mice.

Figure S8. *Expression of ductal and MEC markers in human lacrimal gland (HLG). Related to figure 8.* Frozen sections were stained with the Krt5 (basal ductal and MEC marker), Krt14 (basal ductal and MEC

marker), Krt19 (luminal ductal marker) and SMA (MEC marker) antibodies. As expected, both Krt14 (A-C) and Krt5 (D-F) labeled ductal and MEC cells. Ductal marker Krt19 (G-I) labeled luminal cells and was not expressed in MECs. Abbreviation: *ac* - acini.

Figure S9. *Progression of lineage restriction with LG maturation. Related to Figure 9.* During embryonic development LG epithelium contains multipotent stem/progenitor cells able to give rise to several cell lineages. At the same time αSMA^{+} MEC lineage becomes restricted early in embryonic development. (B) Following birth, lineages become established and the fate of progenitor cell descendants becomes restricted.

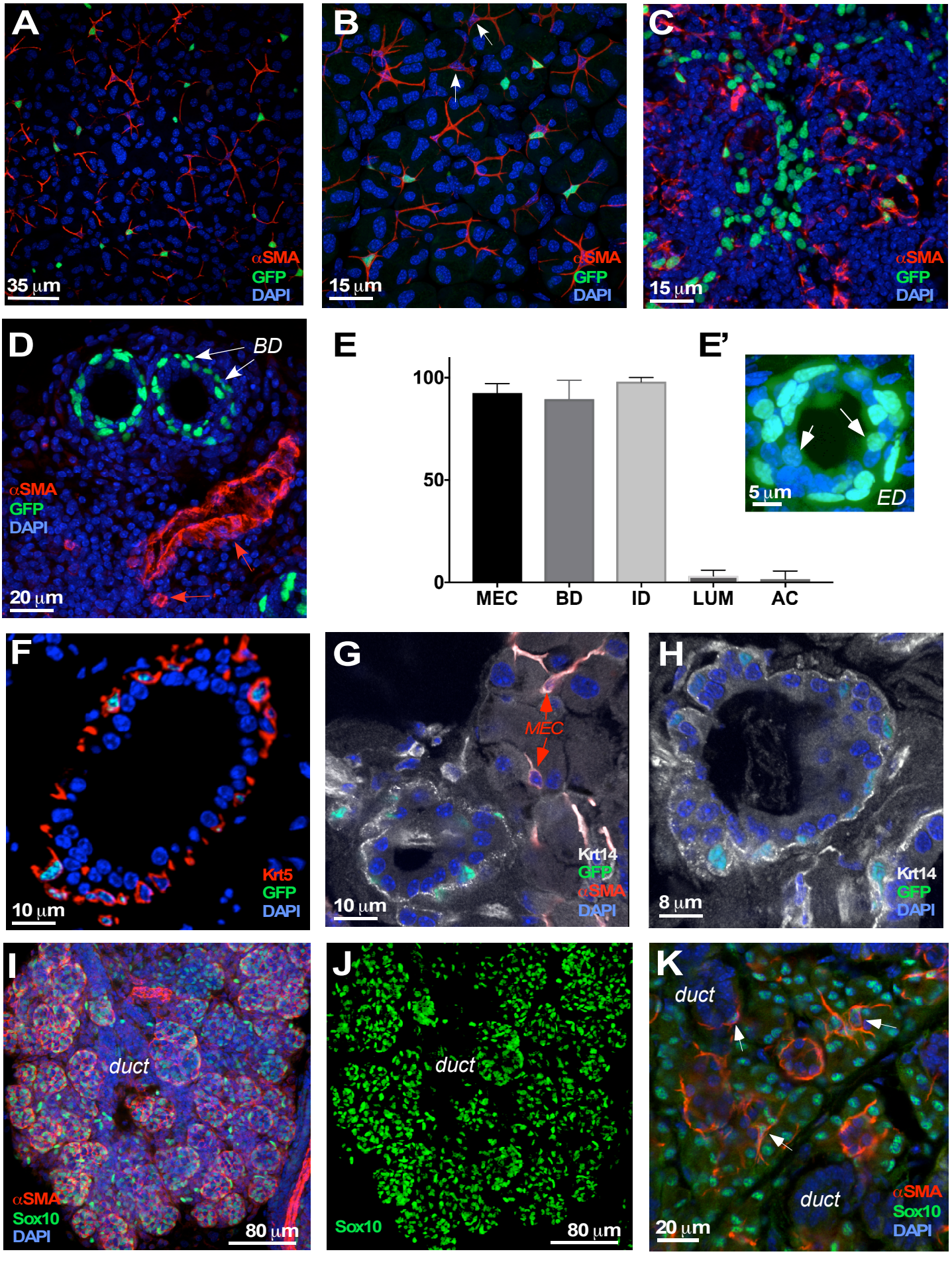

Figure S 1, related to Figure 1.

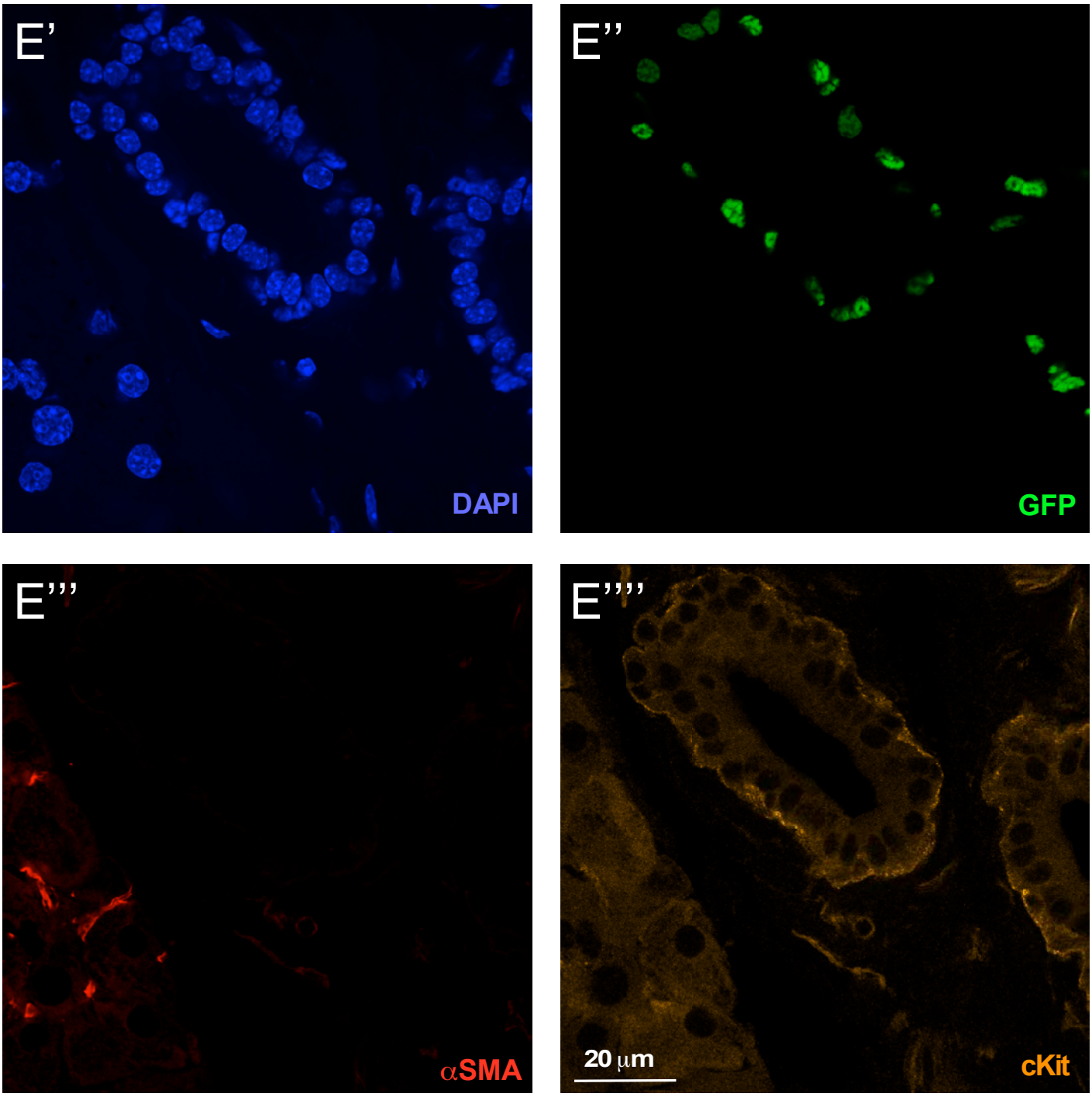

Figure S2, related to Figure 1E.

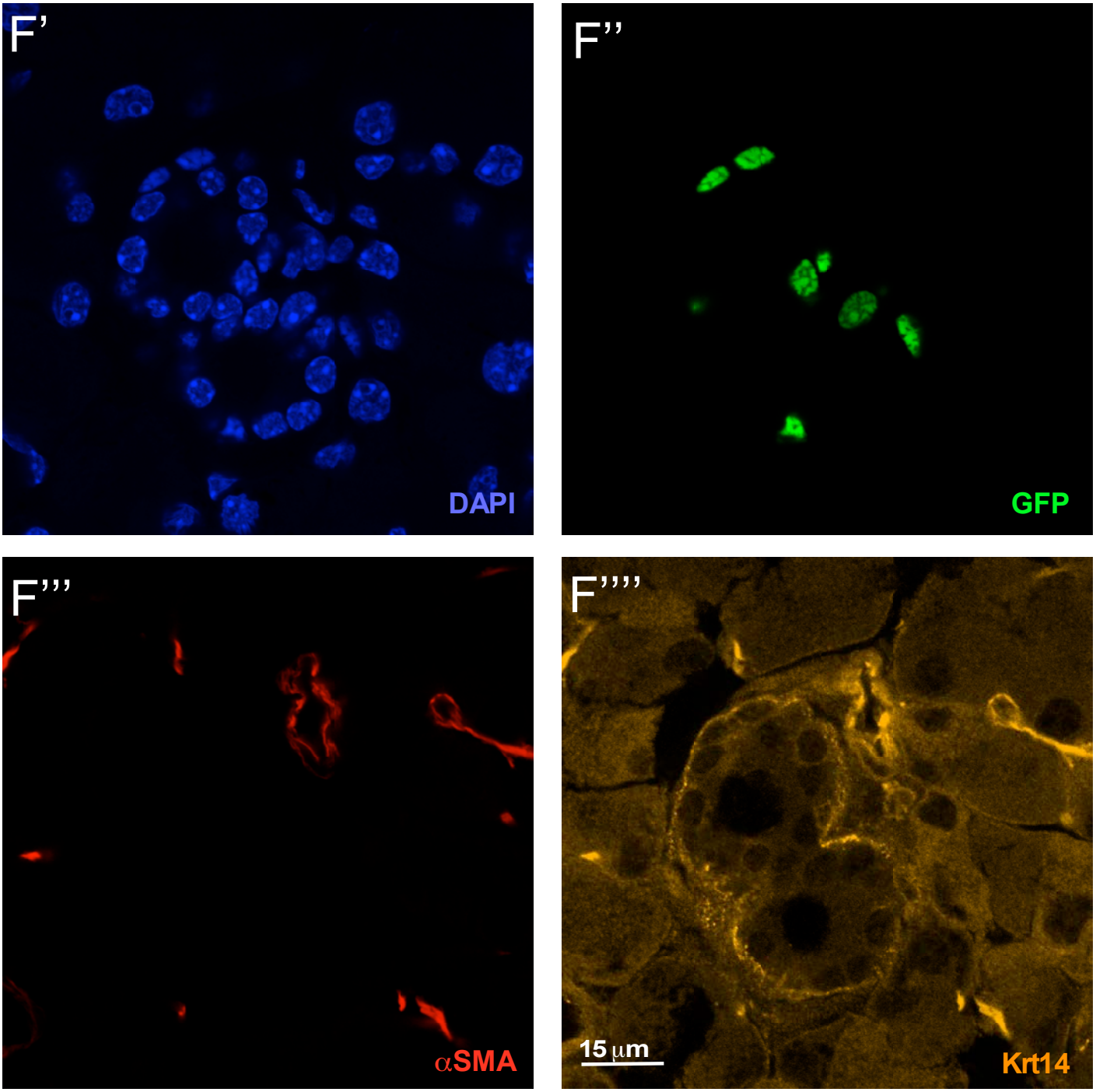

Figure S3 Related to figure 1F.

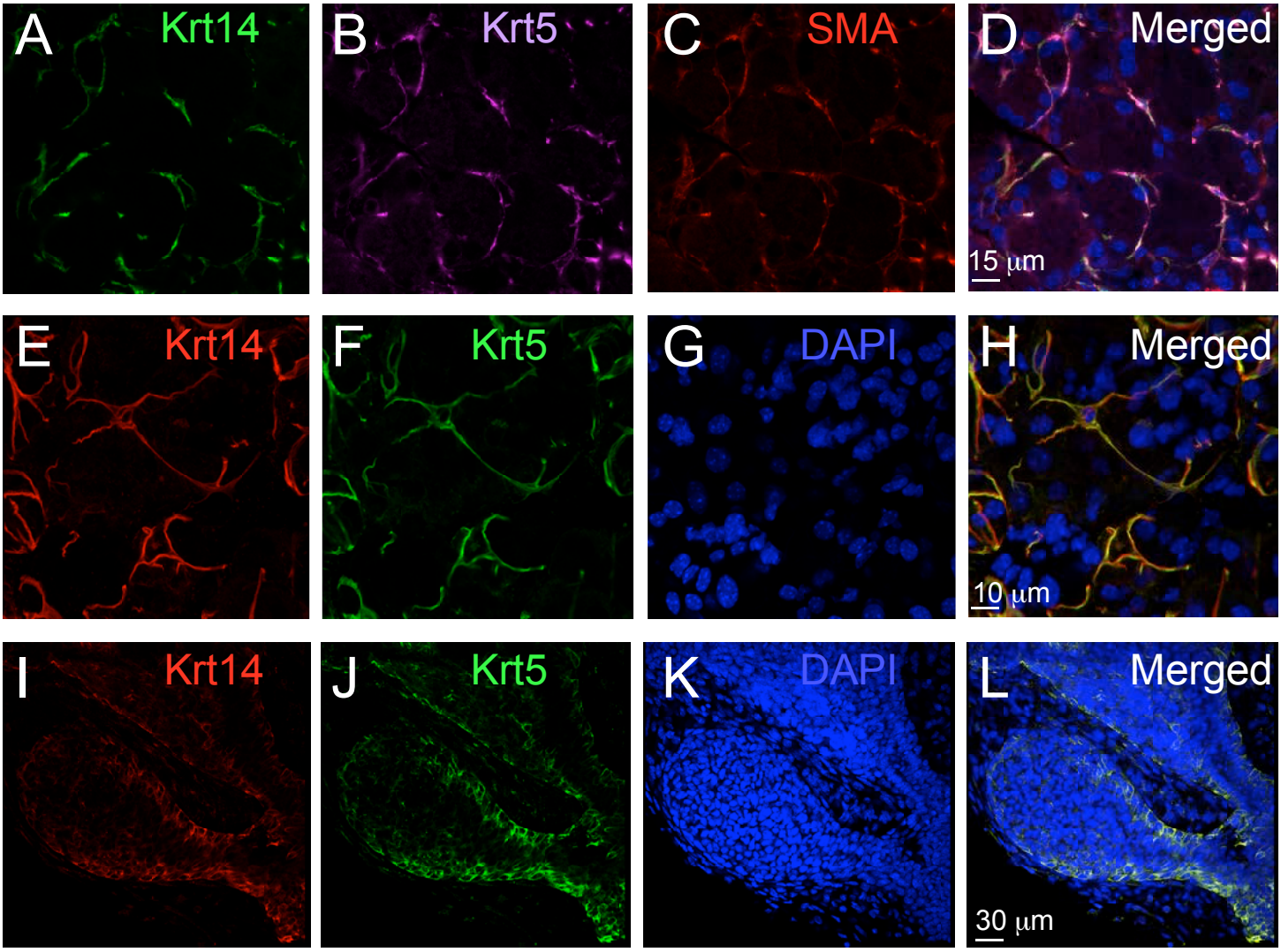

Figure S4, Related to Figure 2.

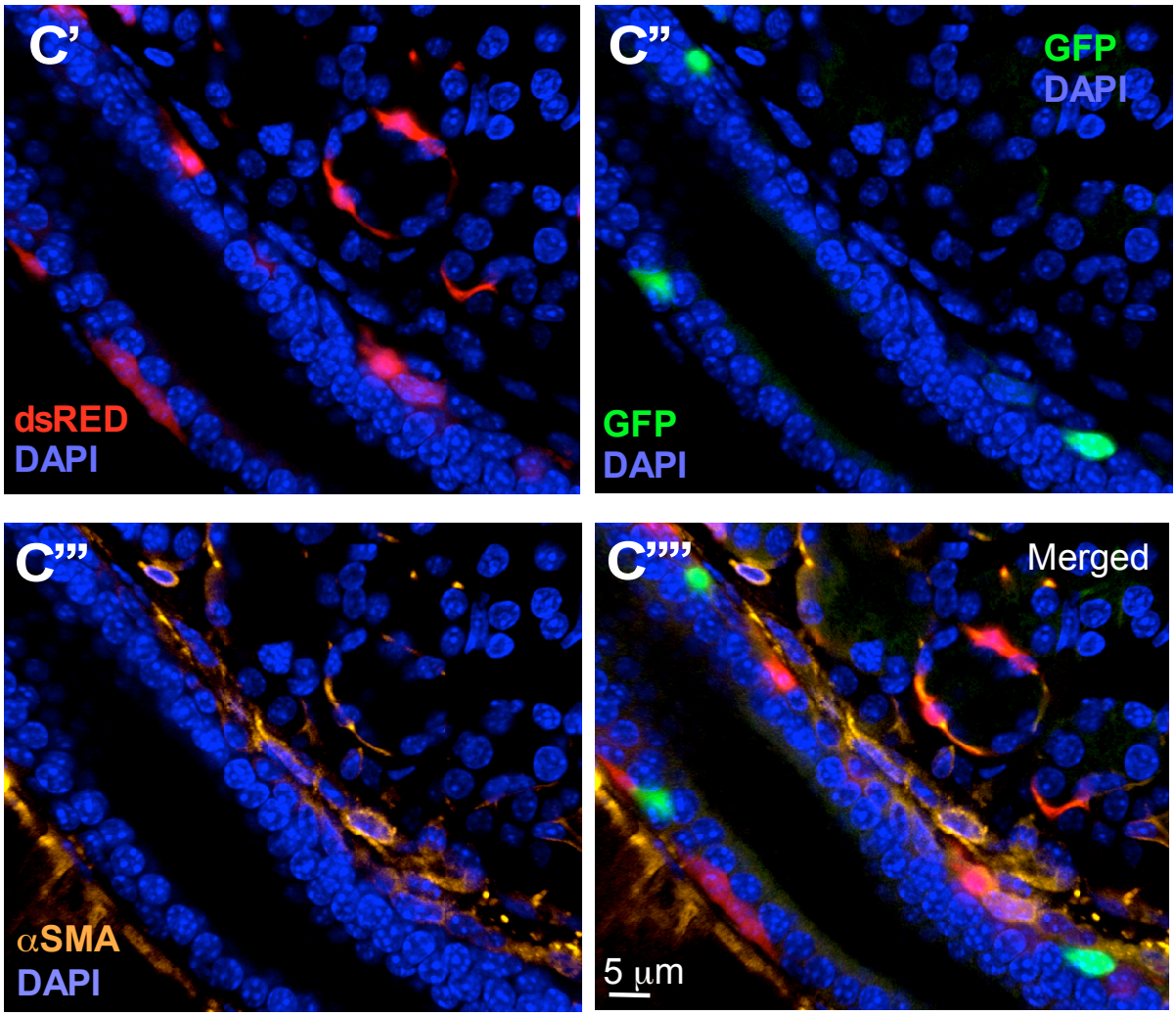

Figure S5, related to Figure 2C.

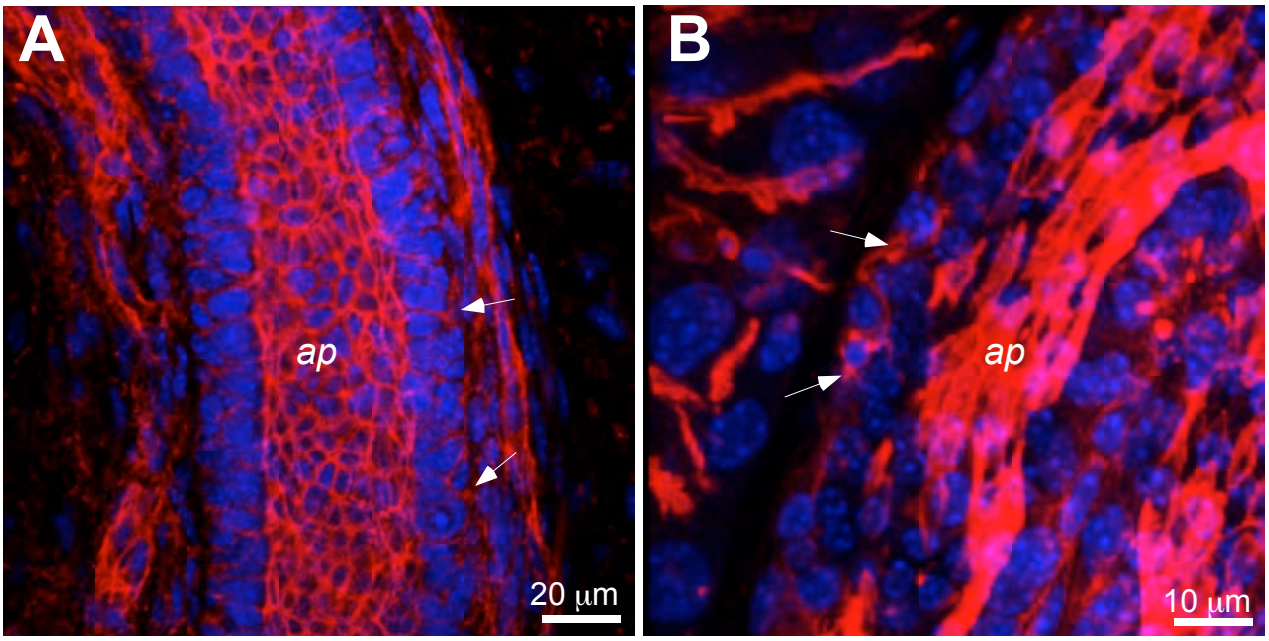

Figure S6, related to Figure 2.

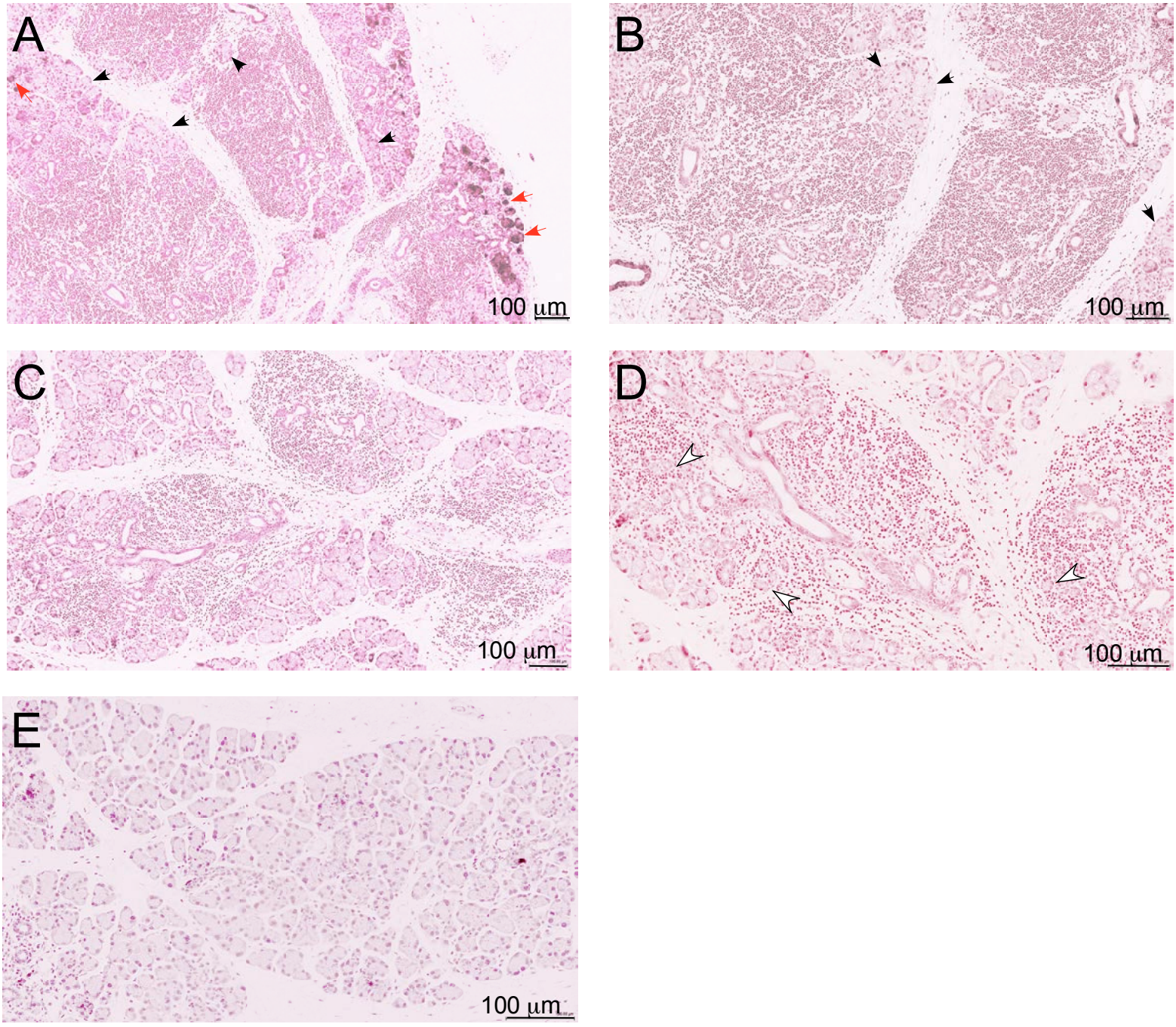

Figure S7, related to Figure 6.

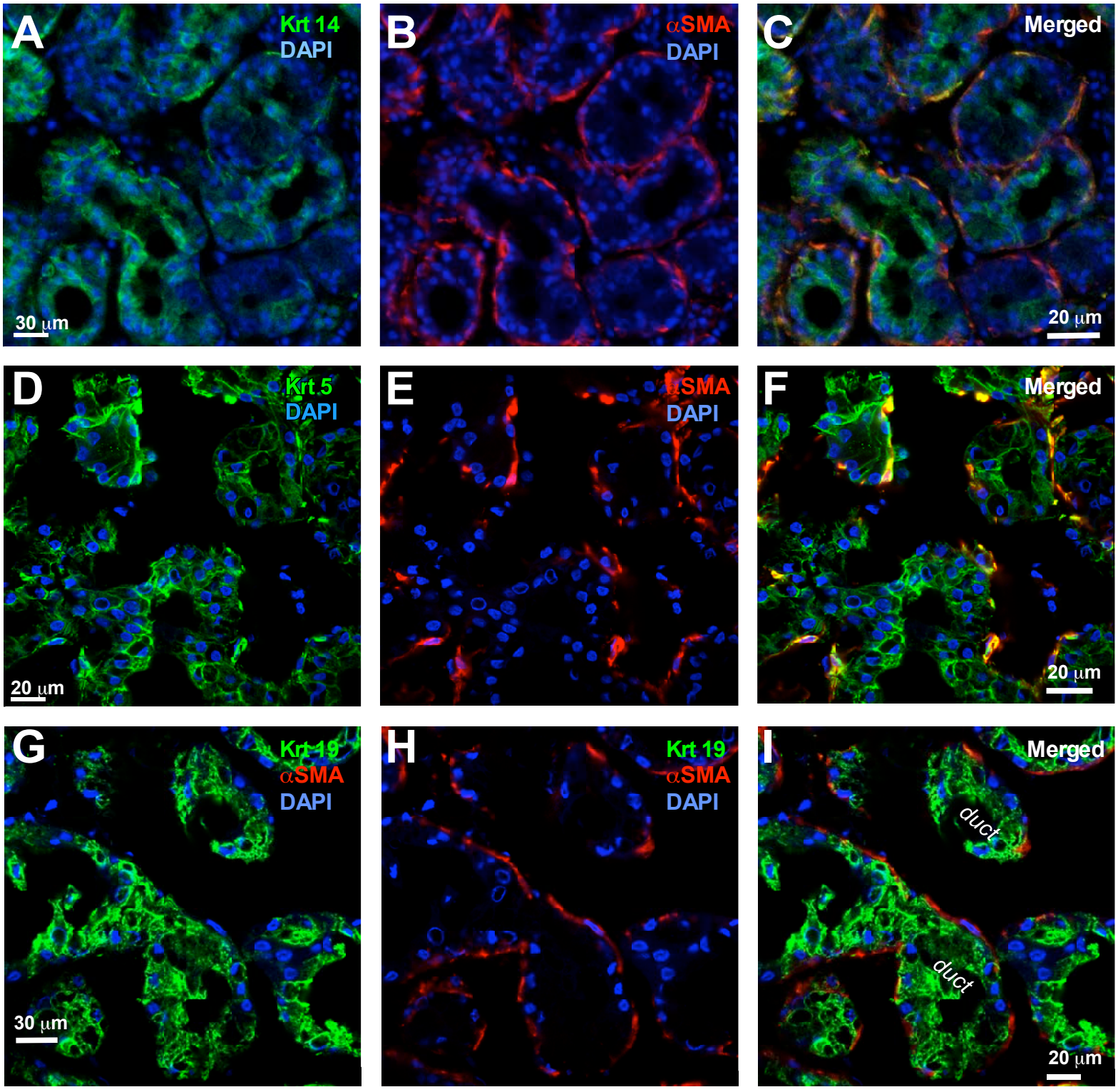

Figure S8, related to Figure 8.

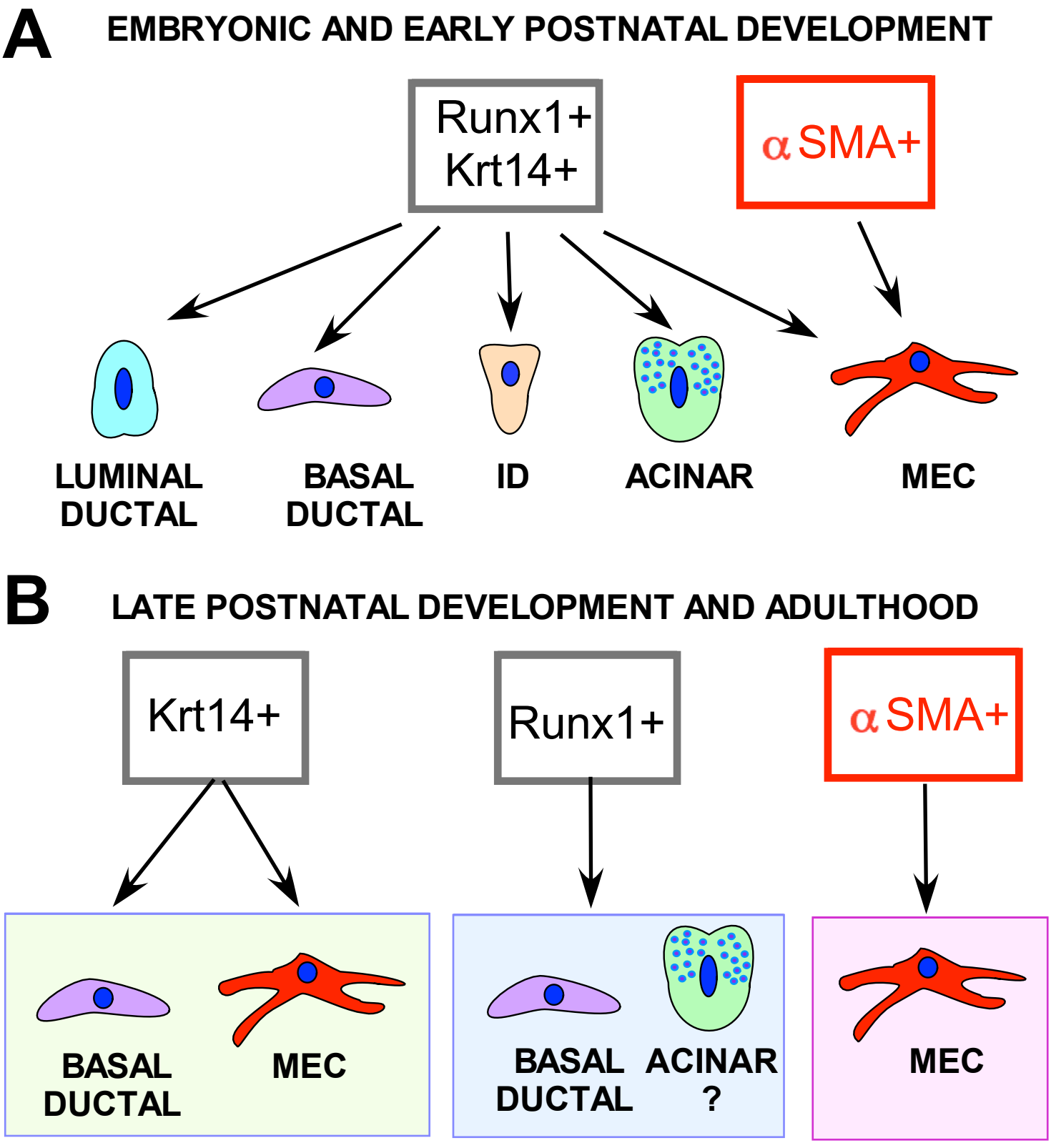

Figure S9, related to Figure 9.

Table S1. Key Reagents and Resources (Related to Figures 1-8, S1-S8 and Transparent Methods)

REAGENT/RESOURSE	SOURCE	IDENTIFIER
Chemicals, kits and recombinant proteins		
4′,6-diamidino-2-phenylindole (DAPI)	Millipore/Sigma	32670
Tamoxifen	Millipore/Sigma	T5648
Progesterone	Millipore/Sigma	P3972
UltraPure™ Low Melting Point Agarose	ThermoFisher Scientific	16520050
Ethanol, Absolute (200 Proof), Molecular Biology Grade	Fisher Scientific	BP 2818,
Xylene (Certified ACS)	Fisher Scientific	X5-500
PBS, Phosphate Buffered Saline, 10X Solution	Fisher Scientific	BP 39920
Sodium Citrate dihydrate (mw: 294.1 g/mol)	Millipore/Sigma	W302600
Citric Acid (mw: 192.1 g/mol)	Millipore/Sigma	251275
DPBS, no calcium, no magnesium	ThermoFisher Scientific	14190144
Gelatin from bovine skin	Millipore/Sigma	G9391
Goat serum	Millipore/Sigma	G9023
2-Methylbutane	Millipore/Sigma	277258
Paraformaldehyde, granular, EM Grade, purified	WVR	100504-160
Tris base	Millipore/Sigma	T1503
Hydrochloric acid	Millipore/Sigma	H1758
Sodium chloride	Millipore/Sigma	1064001000
Sodium hydroxide	Millipore/Sigma	S8045
Flash Phalloidin™ Red 594	Bio-Legend	424203
Fluorescence Mounting Medium	DAKO	S302380
IgG from rabbit serum	Millipore/Sigma	I5006
IgG from mouse serum	Millipore/Sigma	I5381
IgG from goat serum	Millipore/Sigma	I5256
CytoVista Tissue Clearing Reagent	ThermoFisher Scientific	V11300
TWEEN® 20	Millipore/Sigma	P1379
Sodium Chloride 0.9% (Normal Saline), USP, Sterile Grade	Fisher Scientific	Z1376
Hydrogen Peroxide, 30% (Certified ACS)	Fisher Scientific	H325
Methanol (Certified ACS)	Fisher Scientific	A412
Richard-Allan Scientific™ Cytoseal™ XYL	ThermoFisher Scientific	8312-4
Fisherbrand™ Cover Glasses: Rectangles	Fisher Scientific	12-545-M
Thimerosal	Millipore/Sigma	T5125
Casein from bovine milk	Millipore/Sigma	C5890
Phosphate buffered saline	Millipore/Sigma	P4417
Gill Hematoxylin Stain	Fisher Scientific	CS400-1D
VECTASTAIN® Elite ABC-HRP Kit (Peroxidase, Universal)	Vector Laboratories	PK-6200

Vector® NovaRED® Substrate Kit, Peroxidase (HRP)	Vector Laboratories	SK-4800
Tissue-Plus™ O.C.T. Compound	Fisher Scientific	23-730-571
Recombinant Human IL-1 alpha	R&D systems	200-LA-010
Methyl methacrylate	Polysciences	00834.
Butryl methacrylate	Millipore/Sigma	235865
Software		
ImageJ	NIH	N/A
MetaMorph	BioVision technologies	N/A
Prizm 7	GraphPad Software	N/A
Excel	Microsoft	N/A
IMARIS	Oxford Instruments	N/A

Table S2. Primary antibody used for immunoassaying of whole mount preparations and/or frozen, paraffin, plastic sections (Related to Figures 1-6, 8, S1-S5, S8 and Transparent Methods)

Antibody	Antibody information	Whole mount and frozen sections	Paraffin, plastic sections
Sox9 (rabbit monoclonal)	Millipore/Sigma clone 2B10, cat# ZRB5535 (IgG)		1:50
Sox9 (rabbit monoclonal)	Abcam, clone EPR14335-78, cat# ab185966 (IgG)	1:100	1:20
αSMA (mouse monoclonal)	Clone 1A4, ascites fluid, cat# A2547 (IgG2a)	1:400	1:100
RFP (rabbit polyclonal)	Thermo Fisher Scientific, cat# R10367	-	1:1000
Sox10 (goat polyclonal)	Santa Cruz Biotechnology, (N20) Cat# sc-17342	1:100	1:20
Cytokeratin 5 (Krt5) (rabbit monoclonal)	Abcam, clone EP1601Y, cat# ab52635 (IgG)	1:100	1:50
Cytokeratin 5 (Krt5) (mouse monoclonal)	ThermoFisher Scientific, clone 2C2 MA517057 (IgG1)	1:100	
Cytokeratin 14 (Krt14) (mouse monoclonal)	Abcam, clone LL002, cat# ab7800 (IgG3)	1:100	1:50
Cytokeratin 14 antibody, (rabbit monoclonal)	Millipore/Sigma, clone SP53, SAB5500124	1:100	
Thrombospondin 1 (Thbs1) (goat polyclonal)	Santa Cruz Biotechnology Inc., (N-20) cat# sc-12312		1:50
Panx1 (rabbit polyclonal)	Millipore/Sigma, cat# HPA016930	1:100	
Claudin-1 (mouse monoclonal)	Thermo Fisher Scientific, clone 2H10D10, cat# 37-4900 (IgG1)	1:100	
Pax-6 (rabbit polyclonal)	BioLegend, cat# 901301 (previously Covance, cat# PRB-278P)	1:100	
Ser28 phosphorylated histone H3 (rat monoclonal)	Millipore/Sigma, clone HTA28, cat# H9908 (IgG2a)	1:200	

Transparent Materials and Methods

1. Mouse strains and breeding

All experiments were carried out in accordance with the ARVO statement for the Use of Animals in Ophthalmic and Vision Research and were approved by the Scripps Research Institute and the Gavin Herbert Eye Institute Animal Care and Use Committees.

H2B-GFP (Also known as: pTRE-H2BGFP) mice are commercially available from Jackson Laboratories (stock number: 005104) and K5tTA mice were kindly provided by Adam Glick (Diamond et al., 2000). H2B-GFP/K5tTA mice on an FVB background were genotyped and pulsed from P0 to P28 to label all cytokeratin 5^{+} epithelial cells with nuclear green fluorescence protein (GFP). At P28, H2B-GFP/K5tTA mice were fed a doxycycline-containing diet (2g/kg) to initiate the chase period. Krt5^{+} epithelial cells lose 50% of their GFP intensity with every division and quiescent cells retain their GFP label (Parfitt et. al. 2015).

Several mouse lines were used for lineage tracing experiments. Mice expressing tamoxifen (TM)-inducible Cre under control of α-smooth muscle actin (SMA^{CreERT2}) generated by Dr. Kalajzic (Grcevic et al., 2012). αSMA^{CreERT2} mice were crossed with reporter lines, Rosa26-Confetti (Stock No. 017492) and Rosa 26-tdTomato (Stock No 007909, also known as Ai9 (RCL-tdT)) to generate Sma$^{CreERT2/+}$:Rosa26-Confetti$^{fl/+}$ and Sma$^{CreERT2/+}$:Rosa26-tdTomato$^{fl/fl}$. Mice were injected with TM on two consecutive days during embryonic, early postnatal development or adulthood and analyzed following various time periods. Rosa26-Confetti mice were obtained from Jackson Labs.

To study Krt14 cell lineage in the LG, Krt14 $^{CreERT2/+}$:Rosa26-Confetti$^{fl/+}$ mice were injected with TM at the embryonic day 15 (E 15), at one week of postnatal development (P7), six weeks (P36) and ten weeks (P74) of age as previously described (Di Girolamo et al., 2015; Richardson et al., 2017) and tissue from these mice was resected and analyzed at two (P14), four (P30), eight (P60), twenty (P140), and thirty (P210) weeks of age.

A TM-inducible Cre line under the control of the Runx1 promoter (Runx1$^{Mer\text{-}Cre\text{-}Mer/+}$) was generated and generously provided by Dr. Samokhvalov (Samokhvalov et al., 2007) and the RIKEN Center for Life Science Technologies (CLST). This mouse line was used to generate the Runx1$^{Mer\text{-}Cre\text{-}Mer/+}$:Rosa26-Confetti$^{fl/+}$ line.

All Confetti reporter mouse lines used in this study contained the Brainbow 2.1 fluorescent multicolor reporter cassette. All control mice including the TM-inducible reporter mice with no TM injection showed no ectopic cell labeling.

Males and females did not show difference in cell labeling and distribution.

2. Tamoxifen preparation and administration and analysis of clones

Tamoxifen (TM: 1 g) (cat# T5648-1G, Sigma) (also see Table S1 for all reagents and resources) was dissociated in ethanol (2ml) and diluted in filtered corn oil to a final concentration of TM was 20 mg/ml. The solution was vortexed and placed on shaker at 45°C overnight. When completely dissolved, aliquots were stored at -80ºC. TM (1-2 mg/20 g body weight) was administered on 2 consecutive days to adult mice by intraperitoneal injection and to pups by oral gavage.

To label cells during embryonic development TM was administrated by IP to pregnant females at desired times. To neutralize the partial estrogen receptor agonist effects of tamoxifen, which can result in fetal abortions, progesterone (cat# P3972, Millipore/Sigma) (also dissolved in corn oil) was added (at half the total TM dose given, up to 1.5-2 mg of progesterone for single injection). Generally, a single dose of TM 1.5–3 mg was enough to induce reporter expression.

A clone was identified as containing one or several cells with only single fluorescent color. Labeled cells were identified by DAPI staining labeling induced in Rosa26-Confetti reporter mouse by a specific Cre-driver. Ten to twenty random areas (depending on gland size) within each gland were chosen for analysis, from at least three-five biological replicates. Clone sizes of RFP (red cytoplasmic, GFP (green, nuclear), YFP (pale green cytoplasmic), and CFP (blue membrane) labeled cells were analyzed using IMARIS. An average we we able to identify around 100-150 separate clones per gland at each timepoint. Clonal analysis was performed separately within each cellular compartment.

3. Butyl-methyl methacrylate embedding of lacrimal glands

LGs dissected from H2B-GFP/K5tTA mice were immediately fixed in 4% paraformaldehyde (PFA) on ice for plastic embedding. $K14^{CreERT2}$:Confetti mouse lacrimal glands were fixed in 4% PFA up to 59 weeks after TM-induced labeling (69 weeks of age). After fixation, tissues were embedded in 3% low-melting point agarose and dehydrated in 50%, 75%, 95% and then 100% ethanol for 30 minutes each. Butyl-methyl methacrylate (BMMA: Butyl methacrylate, cat# 235865, Millipore/Sigma, St. Louis, MO; Methyl methacrylate, cat# 00834, Polysciences , Warrington, PA) resin infiltration was carried out sequentially in ethanol:BMMA at 2:1, 1:1 and 1:2 ratios for >12 hrs each at 4°C. BMMA-embedded tissues were polymerized under UV light at 4°C for 8 hrs to obtain a plastic block for serial sectioning (Parfitt, 2019).

4. Primary antibodies

The following primary antibodies (Table S2)were used for immunostaining: Sox9 rabbit monoclonal, Sox10 goat polyclonal (N-20), mouse monoclonal α-SMA, Cytokeratin 5 (Krt5) rabbit monoclonal, Cytokeratin 14 (Krt14) mouse monoclonal, and Thrombospondin 1 (Thbs1) goat polyclonal antibody (N-20), Panx1 rabbit polyclonal, Claudin-1 mouse monoclonal), Pax6 rabbit polyclonal, Ser28 phosphorylated histone H3 rat monoclonal, RFP rabbit polyclonal.

5. Immunostaining of BMMA plastic serial-sections

BMMA-embedded lacrimal glands were serially sectioned at 2 µm using a diamond knife attached to an Ultra-microtome (Leica), and the ribbons of sequential serial sections (20 sections/ribbon) were mounted onto 5% gelatin coated slides (2 ribbons/slide) and dried using a slide heater set to 55°C. Slides were then immersed in acetone for 10 mins at room temperature before being rehydrated in 95%, 75% and 50% ethanol. Antigen retrieval was performed for 7 minutes using 1X Sodium Citrate buffer (pH 6.0) in a pressure cooker. After blocking in 5% goat serum, sections were immuno-stained overnight at 4°C with primary antibodies, including anti-RFP to retrieve endogenous fluorescence lost due to ethanol dehydration, Sox9 and αSMA. Tissue sections were then incubated with appropriate secondary antibodies including (Invitrogen) at 37°C for 1 hr.

6. 3-D reconstruction (Immuno-fluorescence tomography)

Fluorescence imaging of serial sections was conducted on a Leica DMI6000B microscope with MetaMorph software for multi-dimensional, mosaic image acquisition. LGs were imaged for GFP before immunostaining was performed to preserve the signal. Mosaic imaging of 3x3 tiles was performed for each section and images were acquired at a pixel resolution of 0.44 µm x 0.44 µm x 2 µm using a 20X/0.75NA objective. Mosaic images of each section were compiled into image stacks using ImageJ software before alignment and 3-D reconstruction using Amira 4.6. The average pixel intensities of GFP+ LRCs was calculated using Amira segmentation software and each LRC was assigned into a category based on their intensity value and level of label retention, with the LRC+++ subpopulation being the most quiescent i.e., LRC+ = 0–100; LRC++ = 100–200; LRC+++ = 200–255. Quantification of total cells and fluorescence intensity of LRCs was carried out using ImageJ's 3-D objects counter.

7. Immunostaining and confocal microscopy

Alternatively LGs dissected from reporter mice (Confetti and Tomato) were fixed with 2% PFA in PBS (pH 7.4) for 20-40 minutes and processed for whole mount immunostaining (see below) or frozen in 2-methylbutane (isopentane; Sigma-Aldrich, St. Louis, MO, USA) cooled by liquid nitrogen, and 15 µm sections were cut with a Microm HM500 cryostat (MICROM International GmbH, Dreieich, Germany). Sections were blocked with 5% goat serum in Tris-buffered saline containing 0.1% Tween 20 (TBST) then incubated with respective primary antibodies at 4°C overnight. Appropriate secondary antibodies were purchased from Thermo Fisher Scientific (Molecular Probes, Waltham, MA). Images were taken using a Zeiss LSM 780 laser scanning confocal microscope (LSCM). The isotype-specific immunoglobulins (normal human, rabbit, goat or mouse IgGs; Millipore/Sigma) or pre-immune serum were used for negative controls. Flash Phalloidin™ Red 594 (Bio-Legend, cat# 424203) has been used to visualize F-actin filaments.

8. Whole mount immunostatining

Permeabilized LG (see above) were separated into lobules and stained with primary antibodies (Table S2) overnight washed 3-4 times with Tris-buffered saline pH 7.5 with 0.1% Tween 20 (TBST) and stained with secondary antibodies for 45-60 mins at room temperature (RT). Where appropriate, nuclei were counter-stained with DAPI. When necessary a CytoVista Tissue Clearing Reagent (V11300, ThermoFisher) has been used for 3D fluorescent imaging of large pieces of LG.

9. Lacrimal gland injury experiments

Female $Sma^{CreERT2/+}$:Rosa26-$tdTomato^{fl/fl}$ mice were injected with TM at P28-30 or at P58-60 to label MECs and ten days later animals were anesthetized, shaved, and control lacrimal glands were injected with vehicle (saline) or were injected with recombinant human interleukin IL-1α (1 µg dissolved in 2 µl of saline), as previously described (Zoukhri et al., 2008). To ensure that the LG is efficiently injured several injections into different LG lobules of each gland were done. Two weeks later, the animals were sacrificed, and the lacrimal glands were dissected and analyzed.

10. Immunohistochemistry on human LG paraffin sections

Human LGs from three donors (all donors were female donors aged 62, 84, and 90 years old) were obtained from Advanced Tissue Services (Phoenix, AZ, USA) or from one of the coauthors (DTT). Tissues were fixed immediately and embedded in paraffin in Scripps histology core facility or processed for frozen sectioning (see above), and 5 µm sections were prepared. Endogenous peroxidase activity on rehydrated sections was blocked by treating slides with 3% hydrogen peroxide in absolute methanol for 30 mins. Antigen retrieval was performed for 40 mins using 0.01 M citrate (pH 6.0) in a humidified heated chamber. Sections were blocked with 5 g/L casein in PBS containing 0.5 g/L thimerosal (Sigma-Aldrich; cat# T5125-25G) for 30 minutes, incubated with primary antibodies, and diluted in casein buffer overnight at 4°C. Sox10, Sox9, Krt5, Krt14, α-SMA, and Thbs1 primary antibodies were used for immunostaining (Table S2). Biotinylated secondary antibodies (Vector Labs, Burlingame, CA) were used at a 1:300 dilution. Visualization was achieved using biotin/avidin-peroxidase (Vector Labs) and Nova Red (Vector Labs). Tissue was counterstained with Gill's hematoxylin (Fisher Scientific, San Diego, CA; CS400).

11. Statistical Analysis and Data Presentation

For experiments using animals, animal numbers reflect group sizes. For non-animal experiments values of n reflect the number of independent experiments performed or number of LG analyzed. Statistical analyses were performed with Prism version 7.00 for Windows (GraphPad Software, La Jolla, CA; www.graphpad.com) or with Excel (Microsoft). Histograms are presented as mean ± SD from a representative experiment or of the normalized data from several experiments. Statistical analysis was performed with unpaired two-tailed Student's *t*-test and two-tailed Fisher's exact tests and a p-value <0.05 was considered statistically significant. Clonal analysis was performed using one-way ANOVA or using Wilcoxon Signed Paired Rank Test.

Supplemental References

Chen, Z., Huang, J., Liu, Y., Dattilo, L.K., Huh, S.H., Ornitz, D., and Beebe, D.C. (2014). FGF signaling activates a Sox9-Sox10 pathway for the formation and branching morphogenesis of mouse ocular glands. Development *141*, 2691-2701.

Di Girolamo, N., Bobba, S., Raviraj, V., Delic, N.C., Slapetova, I., Nicovich, P.R., Halliday, G.M., Wakefield, D., Whan, R., and Lyons, J.G. (2015). Tracing the fate of limbal epithelial progenitor cells in the murine cornea. Stem cells (Dayton, Ohio) *33*, 157-169.

Diamond, I., Owolabi, T., Marco, M., Lam, C., and Glick, A. (2000). Conditional gene expression in the epidermis of transgenic mice using the tetracycline-regulated transactivators tTA and rTA linked to the keratin 5 promoter. J Invest Dermatol *115*, 788-794.

Grcevic, D., Pejda, S., Matthews, B.G., Repic, D., Wang, L., Li, H., Kronenberg, M.S., Jiang, X., Maye, P., Adams, D.J.*, et al.* (2012). In vivo fate mapping identifies mesenchymal progenitor cells. Stem cells (Dayton, Ohio) *30*, 187-196.

Parfitt, G.J. (2019). Immunofluorescence Tomography: High-resolution 3-D reconstruction by serial-sectioning of methacrylate embedded tissues and alignment of 2-D immunofluorescence images. Sci Rep *9*, 1992.

Richardson, A., Lobo, E.P., Delic, N.C., Myerscough, M.R., Lyons, J.G., Wakefield, D., and Di Girolamo, N. (2017). Keratin-14-Positive Precursor Cells Spawn a Population of Migratory Corneal Epithelia that Maintain Tissue Mass throughout Life. Stem Cell Reports *9*, 1081-1096.

Samokhvalov, I.M., Samokhvalova, N.I., and Nishikawa, S. (2007). Cell tracing shows the contribution of the yolk sac to adult haematopoiesis. Nature *446*, 1056-1061.

Zoukhri, D., Fix, A., Alroy, J., and Kublin, C.L. (2008). Mechanisms of murine lacrimal gland repair after experimentally induced inflammation. Invest Ophthalmol Vis Sci *49*, 4399-4406.